Supporting Information

Strategically Hierarchical Improvement of Superprotonic Conductivity in Stable Metal-Organic Framework System

Xiao-Min Li,[a] Jiang Liu,[a] Chen Zhao,[a] Jia-Lin Zhou,[a] Ling Zhao,*[b] Shun-Li Li[a] and Ya-Qian Lan*[a]*

[a]Dr. X.-M. Li, Dr. J. Liu, C. Zhao, J.-L. Zhou, Prof. S.-L. Li, Prof. Y.-Q. Lan
Jiangsu Key Laboratory of Biofunctional Materials, College of Chemistry and Materials Science, Nanjing Normal University, Nanjing 210023, China
E-mail: liuj@njnu.edu.cn
yqlan@njnu.edu.cn

[b]Prof. L. Zhao
Department of Material Science and Chemistry, China University of Geosicences, Wuhan 430074, China
E-mail: zhaoling@cug.edu.cn

Table of Contents

General methods and materials: All reagents used in experiments were analytical grade and used without further purification. All solutions used in experiments were prepared with Millipore water (18.25 MΩ). Zirconium (IV) chloride ($ZrCl_4$) was purchased from ACROS. 2-Aminoterephthalic acid (BDC-NH_2) and poly(vinylidene fluoride) (PVDF) were purchased from Aladdin. Monosodium 2-sulfoterephthalate (BDC-SO_3Na) was purchased from Tokyo Chemical Industry Co. Ltd. Imidazole-2-carboxaldehyde was purchased from Macklin. Zirconyl chloride octahydrate ($ZrOCl_2 \cdot 8H_2O$), Ethanol absolute (CH_3CH_2OH), methanol (CH_3OH), N,N-dimethylformamide (DMF), N,N-dimethylaniline (DMA), formic acid (HCOOH), acetic acid (CH_3COOH) were purchased from Sinopharm Chemical Reagent Co. Ltd. Polyvinylpyrrolidone (PVP) was purchased from Ourchem. Powder X-Ray diffraction (PXRD) patterns were recorded on a D/max 2500VL/PC diffractometer (Japan) equipped with graphite monochromatized Cu-K_α radiation (λ = 1.54060 Å) over the 2θ range of 5-50°. Corresponding work voltage and current is 40 kV and 100 mA, respectively. Thermogravimetric analyses (TGA) was performed by Diamond TG/DTA/DSC of American Perkin-Elmer Company. Nitrogen adsorption-desorption isotherms were measured at 77K on a Quantachrome Instruments Autosorb AS-6B. The samples were activated under N_2 stream at 120 °C for 12 hours. Solid-state ^{13}C CP/MAS NMR spectra were recorded by using a contact time of 3 ms on a Bruker AM-400 NMR spectrometer. H_2O adsorption-desorption isotherms were measured at 298K on a Quantachrome Instruments Autosorb AS-6B. The samples were activated under N_2 stream at 120 °C for 12 hours. Energy dispersive X-ray spectroscopy (EDS) was performed with JSM-5160LV-Vantage typed energy spectrometer. Morphology analysis of the composite materials were examined by a scanning electron microscope (SEM, JSM-7600F) at an acceleration voltage of 10 kV. Transmission electron microscopy (TEM) images were recorded on JEOL-2100F instrument with an acceleration voltage of 200 kV. Elemental mapping was performed with JSM-5160LV-Vantage typed energy spectrometer. Elemental analysis was performed with Flash 2000 from Thermo Fisher. Inductively coupled plasma measurements were performed with Agilent-720.

Synthesis of UiO-66-NH_2: UiO-66-NH_2 was prepared following the method described earlier.[1] $ZrCl_4$ (240 mg) and BDC-NH_2 (186 mg) were dissolved in the DMF (60 mL). Subsequently, the solution was transferred into a 100mL autoclave to heat at 120 °C for 48 hours. The resulting precipitate was collected by centrifugation and washed with DMF and CH_3OH and then immersed in CH_3OH overnight. The solution was then centrifuged to remove liquid and finally dried at 80 °C on vacuum overnight. The final material was obtained.

Synthesis of UiO-66-AS: UiO-66-NH_2 (0.69 g) and BDC-SO_3Na (0.11 g) were dissolved in the DMF (30 mL) and then CH_3COOH (3 mL) was added into the solution. Subsequently, the solution was transferred into a 100 mL three-necked flask and the mixture was heated at 120 °C to reflux for 24 hours. The resulting precipitate was collected by centrifugation and washed with DMF and CH_3OH and then immersed in CH_3OH overnight. The solution was then centrifuged to remove liquid and finally dried at 80 °C on vacuum overnight. The final material was obtained.

Synthesis of IM-UiO-66-AS: The Schiff base grafted UiO-66-AS was synthesized similar to the previous literature. Imidazole-2-carboxaldegyde (67.3 mg) was dissolved in the CH_3CH_2OH (30 mL) and then UiO-66-AS (235 mg) was added into the solution. Subsequently, the solution was transferred into a 100 mL three-necked flask and the mixture was heated at 80 °C to reflux for 24 hours. The resulting precipitate was collected by centrifugation and washed with CH_3CH_2OH. After drying at 80 °C on vacuum overnight, the final material was obtained.

Synthesis of UiO-66-SO_3H: UiO-66-SO_3H was prepared following the method described earlier.[2] $ZrOCl_2 \cdot 8H_2O$ (1 g) and BDC-SO_3Na (0.83 g) were dissolved in the DMA (30 mL) and HCOOH (11.7 mL, 0.031 mol). Subsequently, the solution was transferred into a 100 mL autoclave to heat at 150 °C for 24 hours. The resulting precipitate was collected by centrifugation and washed with DMA, H_2O and CH_3OH and then immersed in CH_3OH overnight. The solution was then centrifuged to remove liquid and finally dried at 80 °C on vacuum overnight. The final material was obtained.

Synthesis of UiO-66-NH_2-IM: UiO-66-NH_2-IM was prepared following the method described earlier.[3] Imidazole-2-carboxaldegyde (67.3 mg) was dissolved in the

CH_3CH_2OH (30 mL) and then UiO-66-NH_2 (235 mg) was added into the solution. Subsequently, the solution was transferred into a 100 mL three-necked flask and the mixture was heated at 80 °C to reflux for 24 hours. The resulting precipitate was collected by centrifugation and washed with CH_3CH_2OH. After drying at 80 °C on vacuum overnight, the final material was obtained.

Synthesis of IM-UiO-66-AS@PP membrane: IM-UiO-66-AS (120 mg) was sonically dispersed in the DMF (3 mL) for 1 hour. Subsequently, PVDF (24 mg) and PVP (56 mg) were added into the above dispersion and then the mixture was stirred at room temperature for 4 hours to get a homogeneous jelly, which was poured into a mold with polytetrafluoroethylene (PTFE). After drying at 80 °C for 4 hours, the membrane was obtained. When the temperature dropped to room temperature, the membrane was taken carefully off the mold and then washed with distilled water. Finally, the membrane was dried in air for next measurements.

Synthesis of UiO-66-NH_2@PP membrane: UiO-66-NH_2 (120 mg) was sonically dispersed in the DMF (3 mL) for 1 hour. Subsequently, PVDF (24 mg) and PVP (56 mg) were added into the above dispersion and then the mixture was stirred at room temperature for 4 hours to get a homogeneous jelly, which was poured into a mold with polytetrafluoroethylene (PTFE). After drying at 80 °C for 4 hours, the membrane was obtained. When the temperature dropped to room temperature, the membrane was taken carefully off the mold and then washed with distilled water. Finally, the membrane was dried in air for next measurements.

Synthesis of UiO-66-AS@PP membrane: UiO-66-AS (120 mg) was sonically dispersed in the DMF (3 mL) for 1 hour. Subsequently, PVDF (24 mg) and PVP (56 mg) were added into the above dispersion and then the mixture was stirred at room temperature for 4 hours to get a homogeneous jelly, which was poured into a mold with polytetrafluoroethylene (PTFE). After drying at 80 °C for 4 hours, the membrane was obtained. When the temperature dropped to room temperature, the membrane was taken carefully off the mold and then washed with distilled water. Finally, the membrane was dried in air for next measurements.

Synthesis of UiO-66-SO_3H@PP membrane: UiO-66-SO_3H (120 mg) was sonically dispersed in the DMF (3 mL) for 1 hour. Subsequently, PVDF (24 mg) and PVP (56 mg) were added into the above dispersion and then the mixture was stirred at room temperature for 4 hours to get a homogeneous jelly, which was poured into a mold with polytetrafluoroethylene (PTFE). After drying at 80 °C for 4 hours, the membrane was obtained. When the temperature dropped to room temperature, the membrane was taken carefully off the mold and then washed with distilled water. Finally, the membrane was dried in air for next measurements.

Synthesis of UiO-66-NH_2-IM@PP membrane: UiO-66-NH_2-IM (120 mg) was sonically dispersed in the DMF (3 mL) for 1 hour. Subsequently, PVDF (24 mg) and PVP (56 mg) were added into the above dispersion and then the mixture was stirred at room temperature for 4 hours to get a homogeneous jelly, which was poured into a mold with polytetrafluoroethylene (PTFE). After drying at 80 °C for 4 hours, the membrane was obtained. When the temperature dropped to room temperature, the membrane was taken carefully off the mold and then washed with distilled water. Finally, the membrane was dried in air for next measurements.

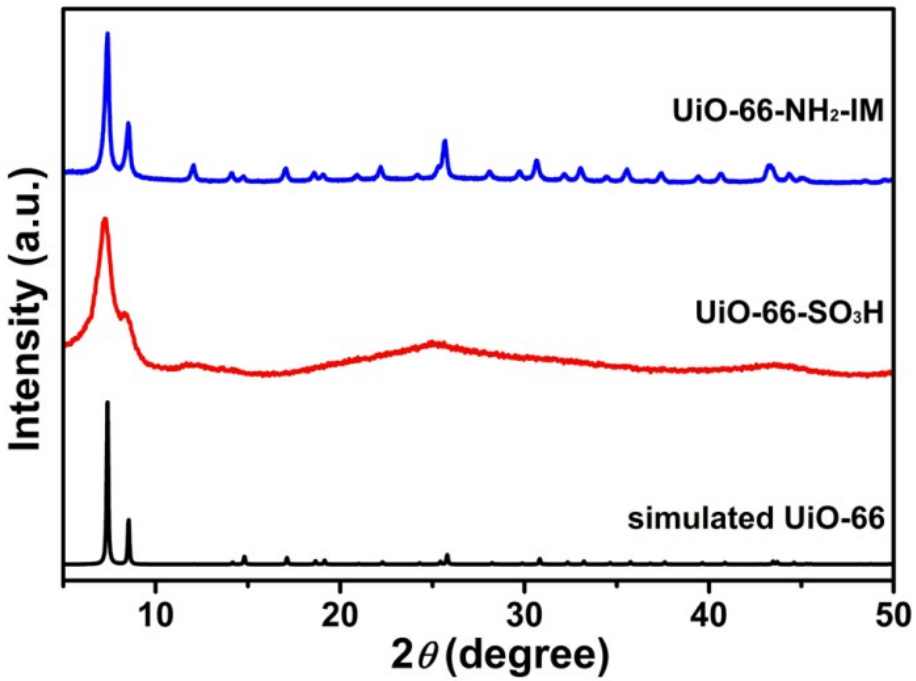

Figure S1. PXRD patterns of simulated UiO-66 (black), as-synthesized UiO-66-SO_3H (red) and as-synthesized UiO-66-NH_2-IM (blue).

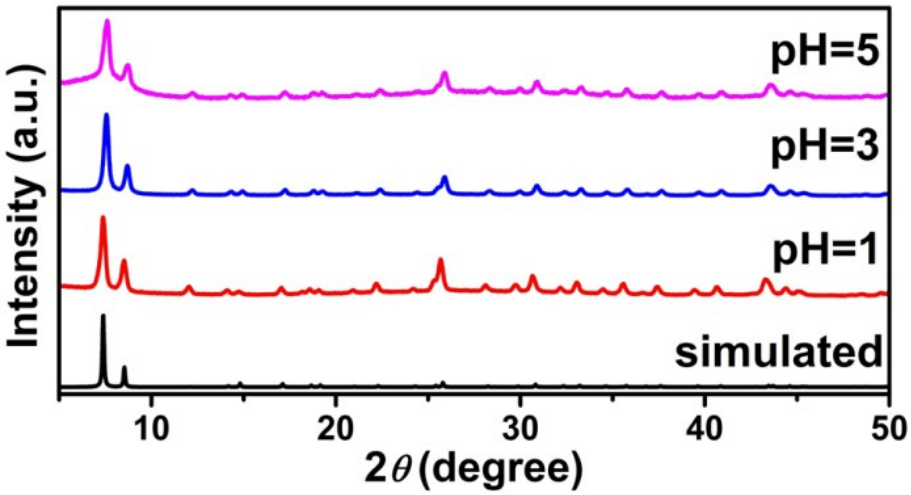

Figure S2. PXRD patterns after soaking in sulfuric acid solution with different pH values of IM-UiO-66-AS.

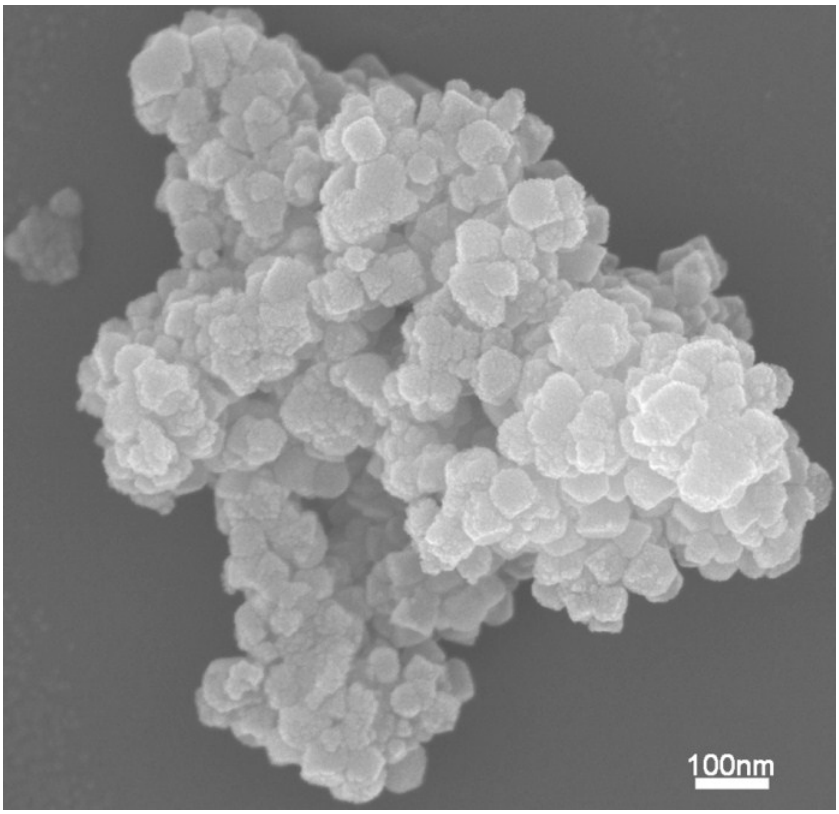

Figure S3. SEM image of as-synthesized UiO-66-NH_2.

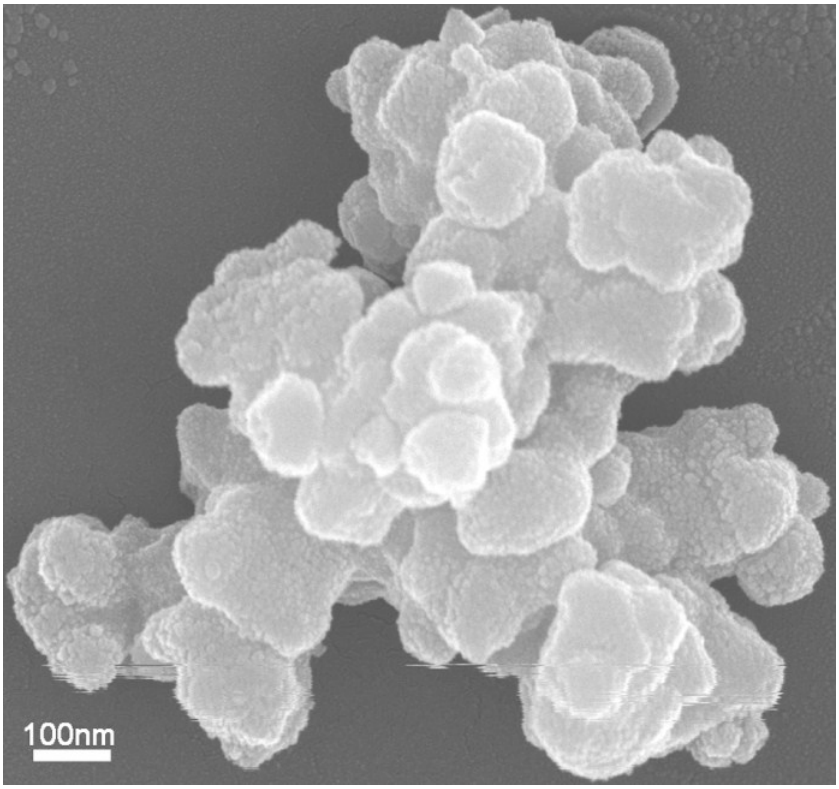

Figure S4. SEM image of as-synthesized UiO-66-AS.

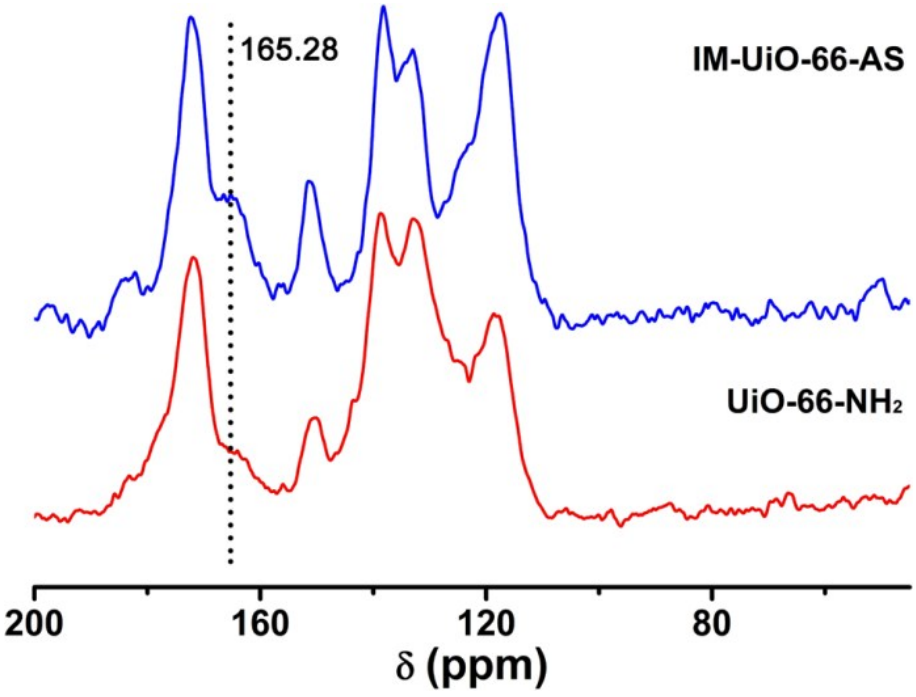

Figure S5. Solid state ^{13}C CP/MAS NMR spectra of UiO-66-NH_2 (red) and IM-UiO-66-AS (blue).

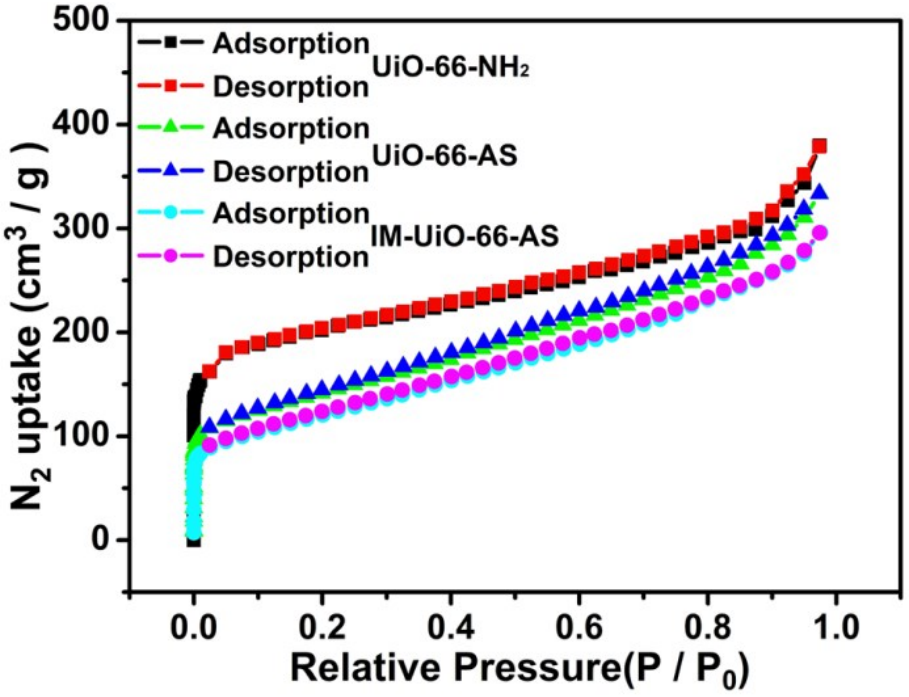

Figure S6. N_2 adsorption-desorption isotherms of as-synthesized UiO-66-NH_2 (black and red), as-synthesized UiO-66-AS (green and blue) and as-synthesized IM-UiO-66-AS (cyan and magenta) measured at 77K.

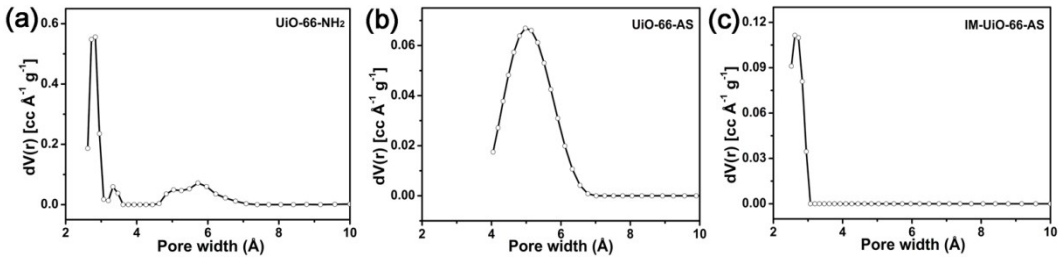

Figure S7. Pore size distribution curves of (a) UiO-66-NH_2, (b) UiO-66-AS and (c) IM-UiO-66-AS.

Table S1. The BET surface area and specific pore volume (V_p) for UiO-66-NH_2, UiO-66-AS and IM-UiO-66-AS.

Material	BET surface area / m^2 g^{-1}	V_p / cm^3 g^{-1}
UiO-66-NH_2	714.62	0.636
UiO-66-AS	386.69	0.530
IM-UiO-66-AS	329.72	0.432

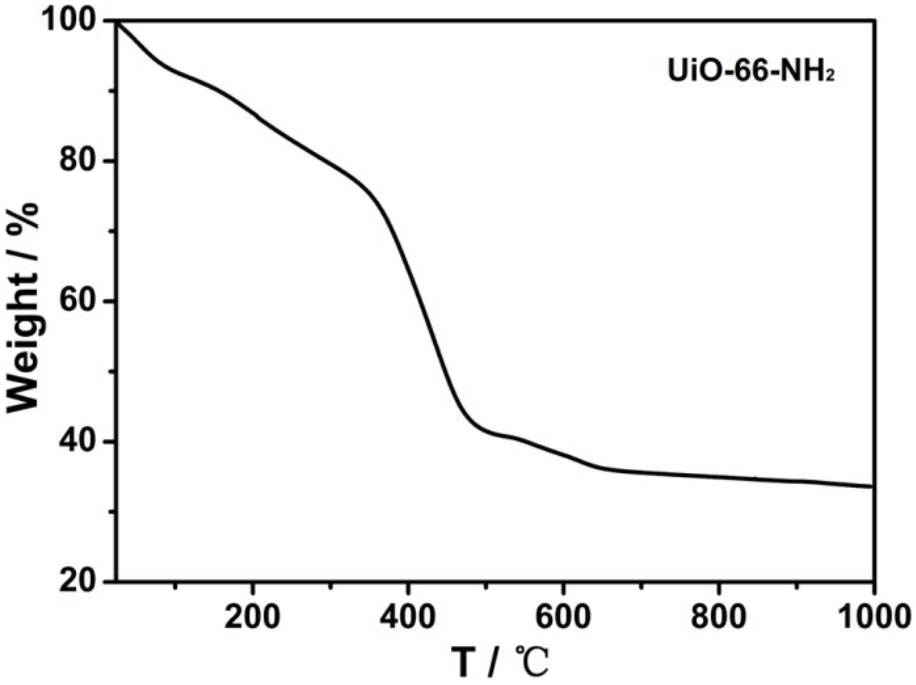

Figure S8. TGA traces of as-synthesized UiO-66-NH_2.

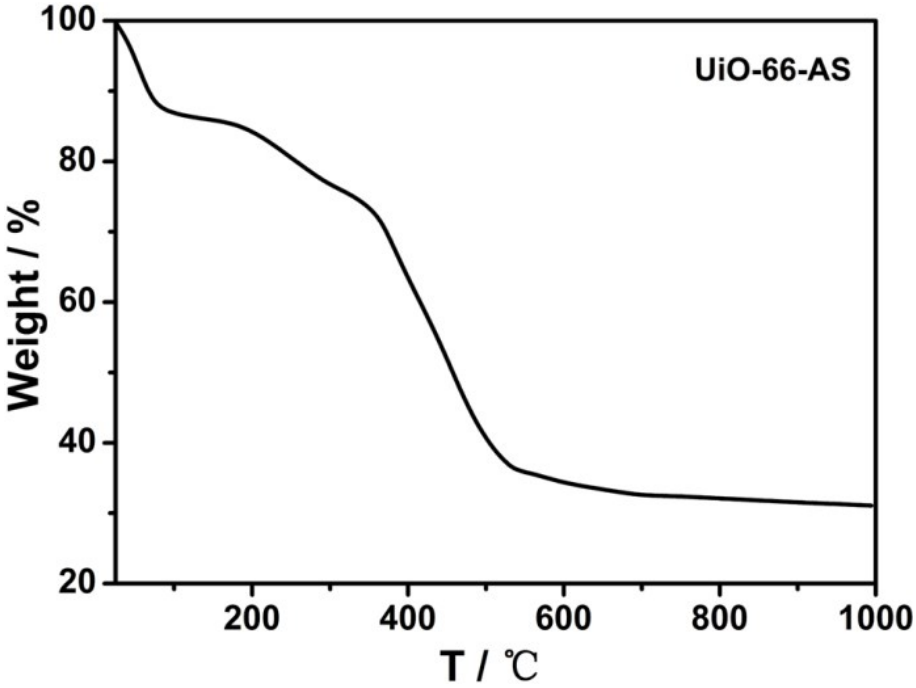

Figure S9. TGA traces of as-synthesized UiO-66-AS.

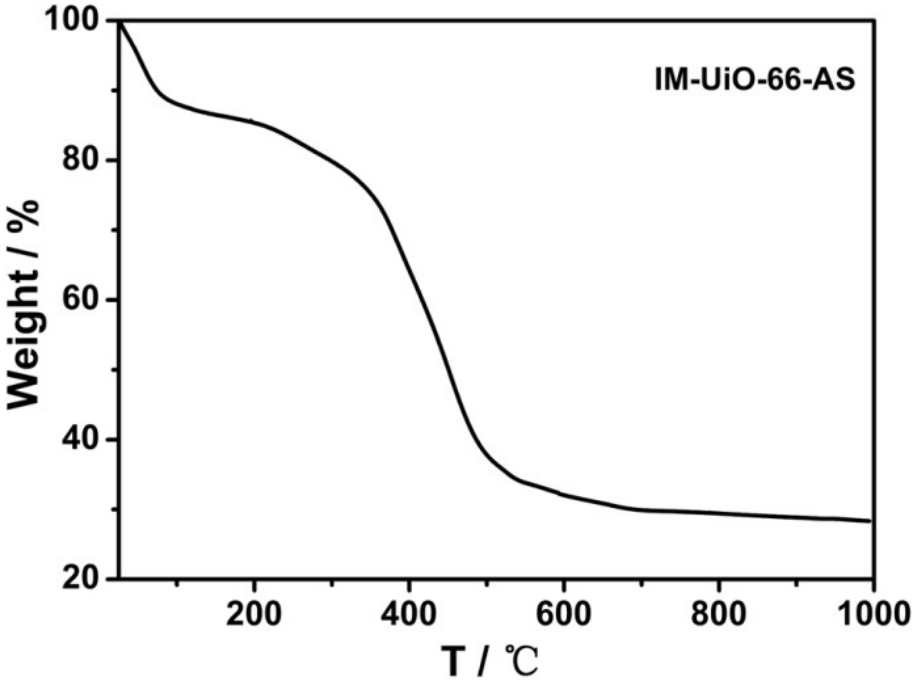

Figure S10. TGA traces of as-synthesized IM-UiO-66-AS.

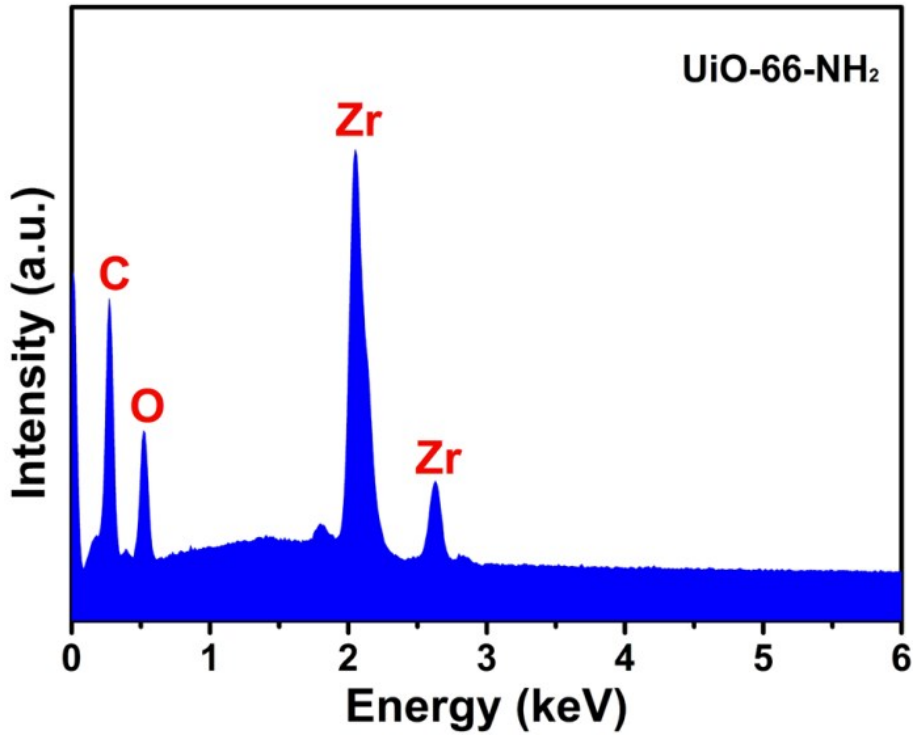

Figure S11. EDX spectrum of UiO-66-NH_2.

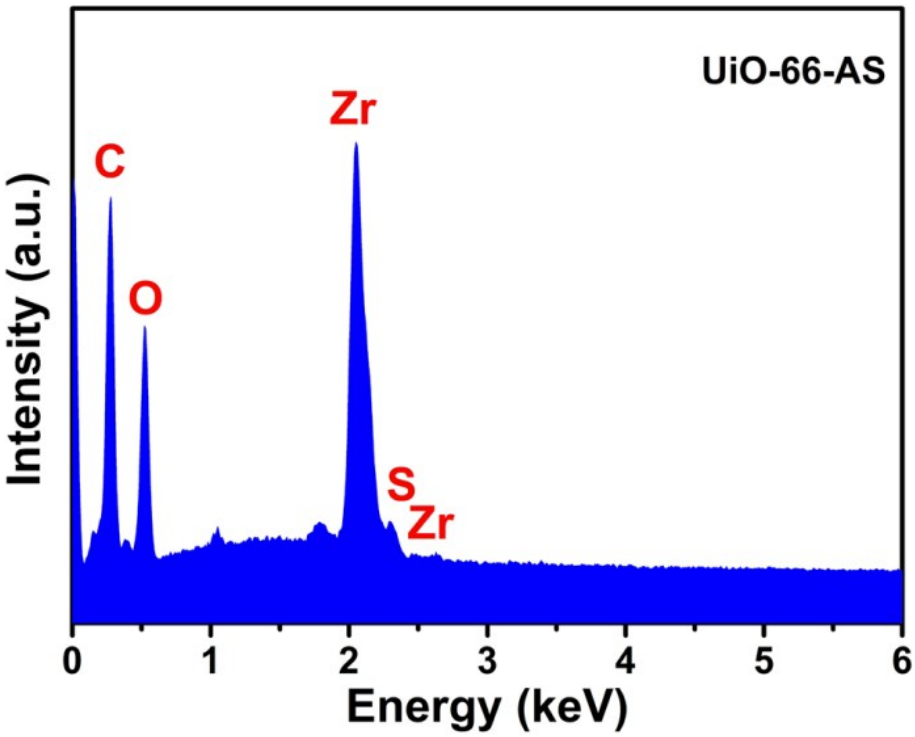

Figure S12. EDX spectrum of UiO-66-AS.

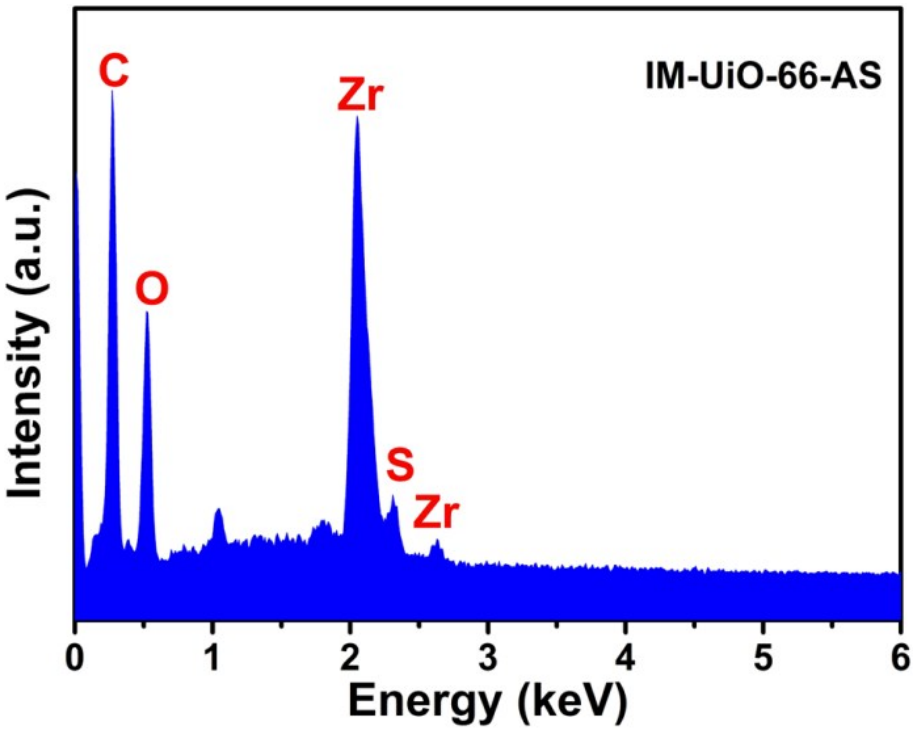

Figure S13. EDX spectrum of IM-UiO-66-AS.

Table S2. Mass percents of materials determined by elemental analysis measurements.

Material	C (wt %)	H (wt %)	N (wt %)	S (wt %)

UiO-66-NH_2	32.59	1.961	4.59	0
UiO-66-AS	31.28	1.829	3.64	2.211
IM-UiO-66-AS	35.12	1.892	8.91	1.864

Table S3. Mass percents of materials determined by inductively coupled plasma measurements.

Material	Zr (wt %)	S (wt %)
UiO-66-NH_2	30.29	0
UiO-66-AS	28.21	2.17
IM-UiO-66-AS	24.47	1.88

Proton conductivity characterization

As far as sample preparation is concerned, firstly, the powder samples were put into a self-made mold with a radius of 0.2 cm for compression to obtain circular pellets and their thicknesses were determined by a vernier caliper. Secondly, the pellets were coated with silver glue on top and bottom sides and dried naturally in air. Thirdly, the pellets were fixed on the sample holders with gold wires. The proton conductivities of pellets were measured using a quasi-four-probe method with an impedance/gain-phase analyzer (Solartron S1 1260) ranging the frequency from 1 Hz to 1 MHz with an input voltage of 300 mV. As for the membrane, it was cut into a rectangle and sandwiched between two gold pieces. The measurements were executed at 30 °C and under different relative humidities (40% to 98% RH) and under 98% RH and at different temperatures (30 to 80 °C), respectively. And then the values of proton conductivities were calculated using the following equation

$$\sigma = \frac{l}{SR}$$

where σ, l, S and R mean the conductivity (S cm^{-1}), the thickness (cm) of the pellet, the cross-sectional area (cm^2) of the pellet and the bulk resistance (Ω), respectively. The

activation energy (E_a) was calculated from the following equation

$$\ln \sigma_T = \ln \sigma_0 - \frac{E_a}{KT} \qquad (K = 8.6\times10^{-5}\ \text{eV/K})$$

where σ, K and T mean the conductivity (S cm^{-1}), the Boltzmann constant (eV/K) and the temperature (K), respectively. ZView software was used to get bulk resistance by fitting the semicircle of Nyquist plots and the values of conductivity and activated energy were obtained by calculation following the above equations.

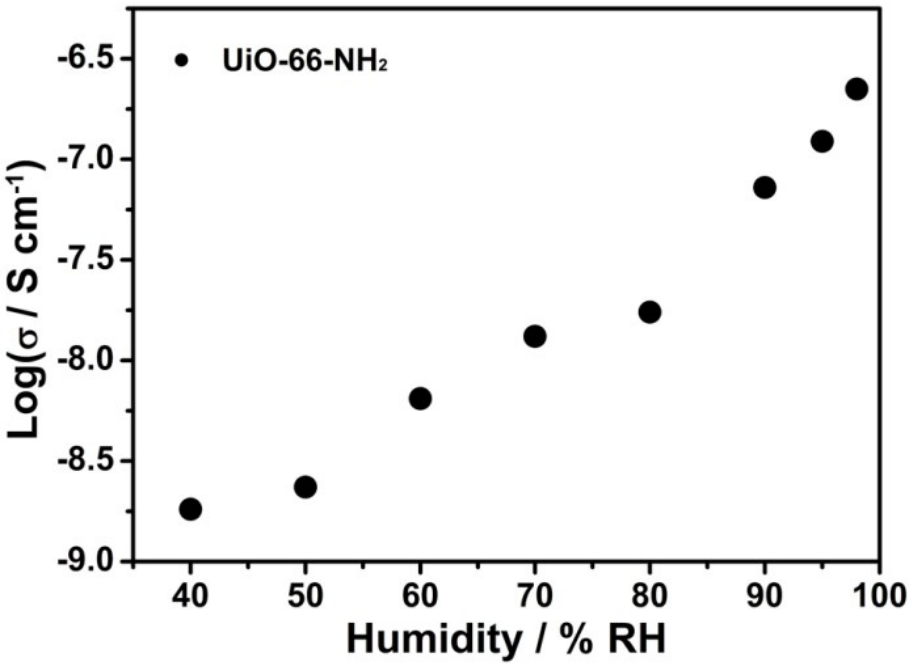

Figure S14. Log-scaled proton conductivities of UiO-66-NH_2 at 30 °C and different humidities variation from 40% to 98% RH.

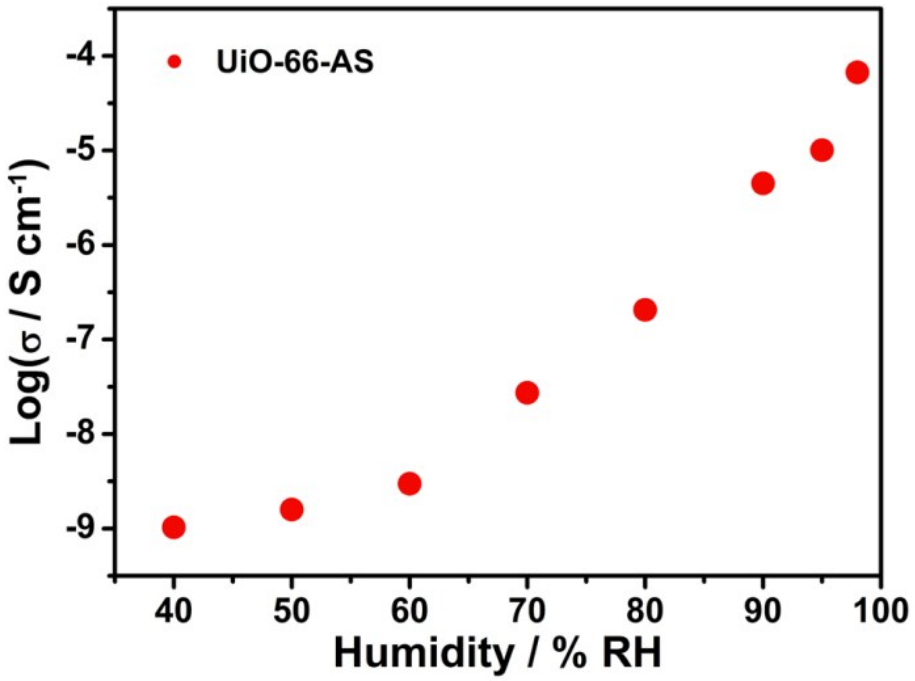

Figure S15. Log-scaled proton conductivities of UiO-66-AS at 30 °C and different humidities variation from 40% to 98% RH.

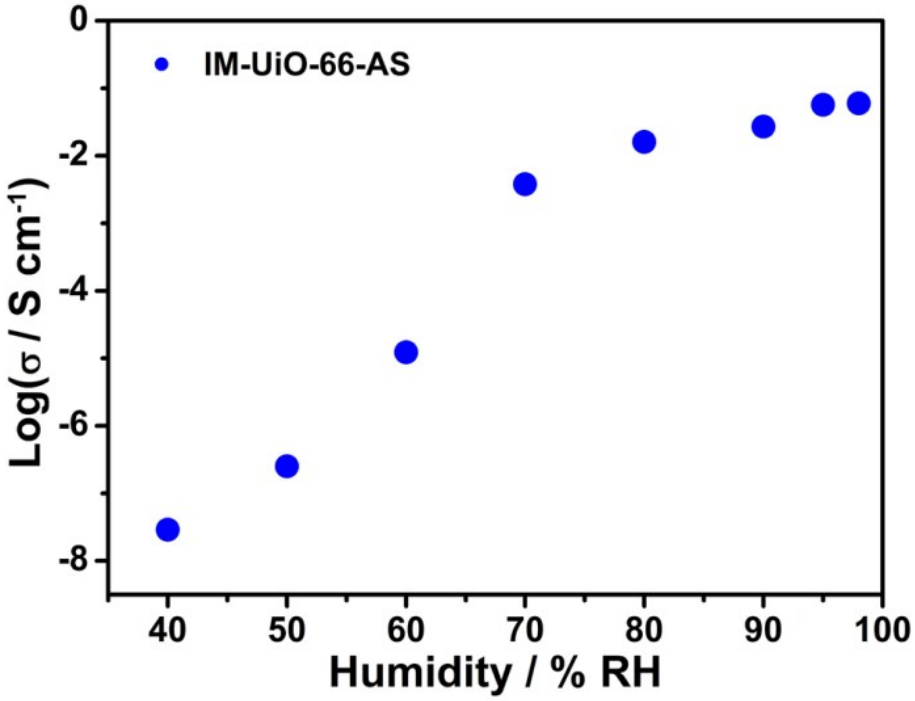

Figure S16. Log-scaled proton conductivities of IM-UiO-66-AS at 30 °C and different humidities variation from 40% to 98% RH.

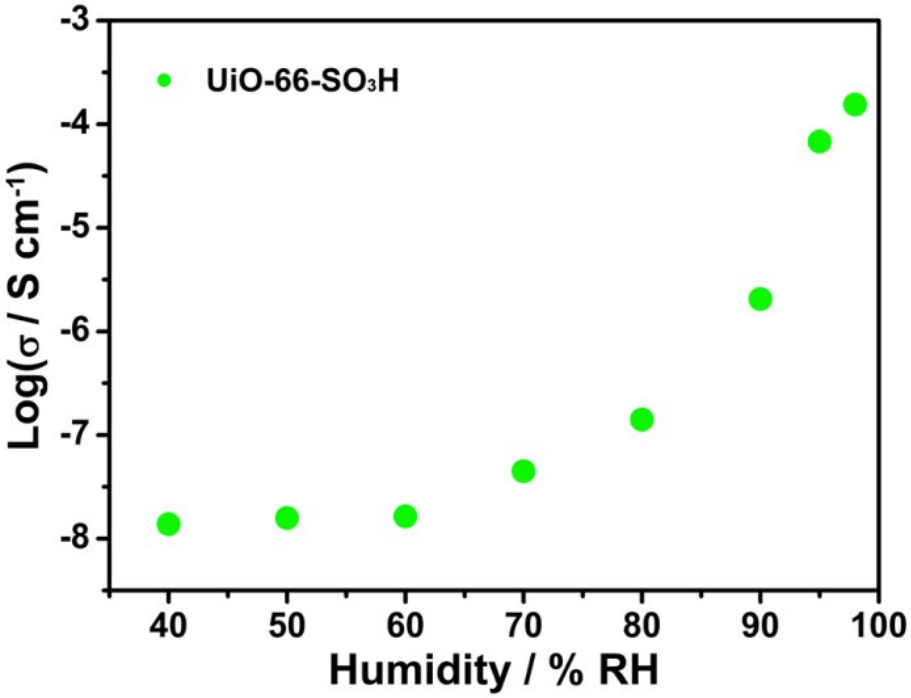

Figure S17. Log-scaled proton conductivities of UiO-66-SO_3H at 30 °C and different humidities variation from 40% to 98% RH.

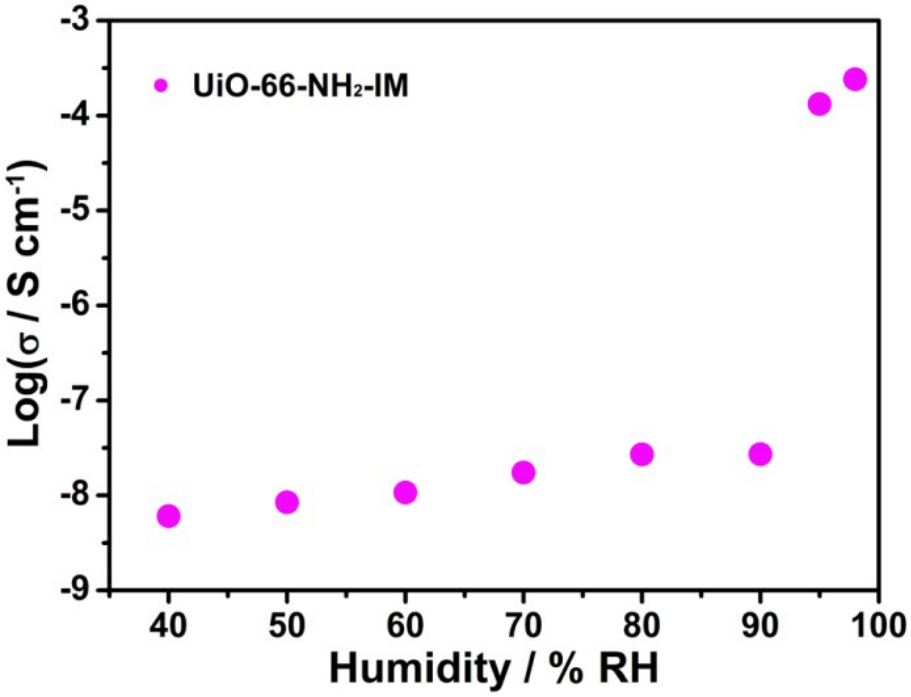

Figure S18. Log-scaled proton conductivities of UiO-66-NH_2-IM at 30 °C and different humidities variation from 40% to 98% RH.

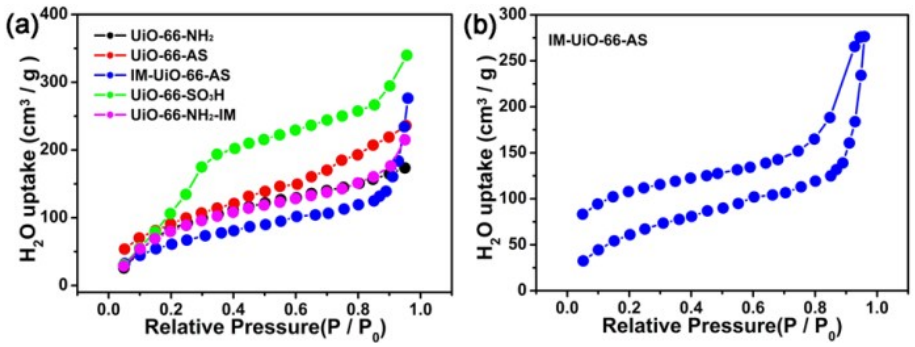

Figure S19. (a) H_2O adsorption isotherms of UiO-66-NH_2 (black), UiO-66-AS (red), IM-UiO-66-AS (blue), UiO-66-SO_3H (green) and UiO-66-NH_2-IM (magenta) measured at 298K, (b) H_2O adsorption-desorption isotherm of IM-UiO-66-AS.

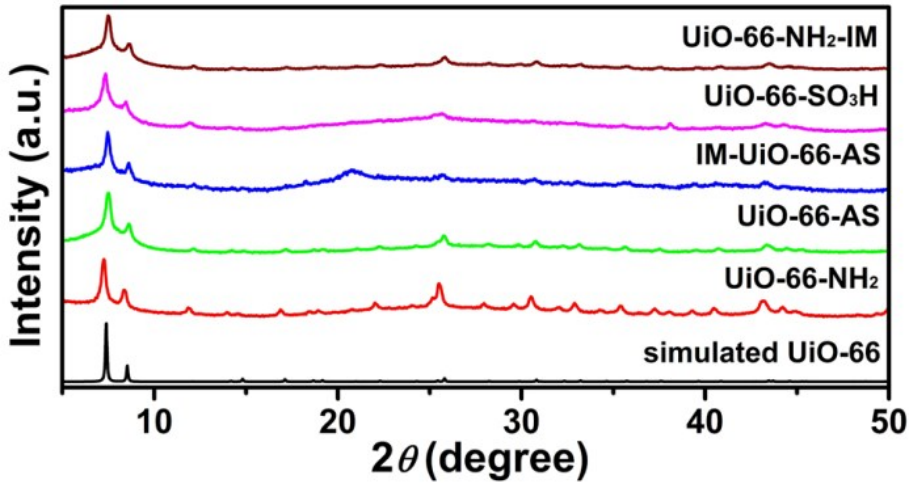

Figure S20. PXRD patterns of simulated UiO-66 (black) and UiO-66-NH_2 (red), UiO-66-AS (green), IM-UiO-66-AS (blue), UiO-66-SO_3H (magenta) and UiO-66-NH_2-IM (wine) undergoing water adsorption measurements.

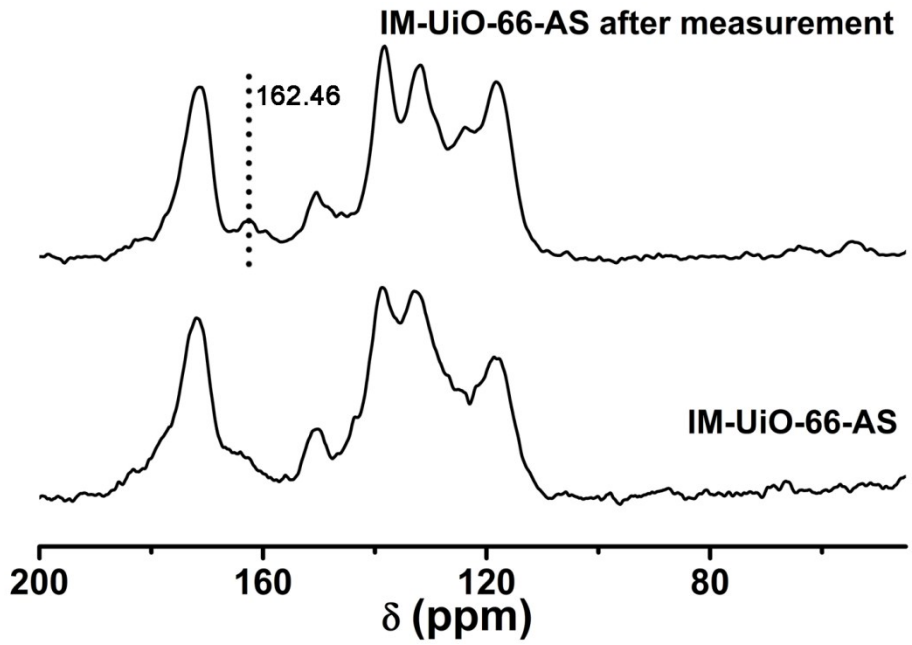

Figure S21. Solid state ^{13}C CP/MAS NMR spectrum of IM-UiO-66-AS undergoing water adsorption measurement.

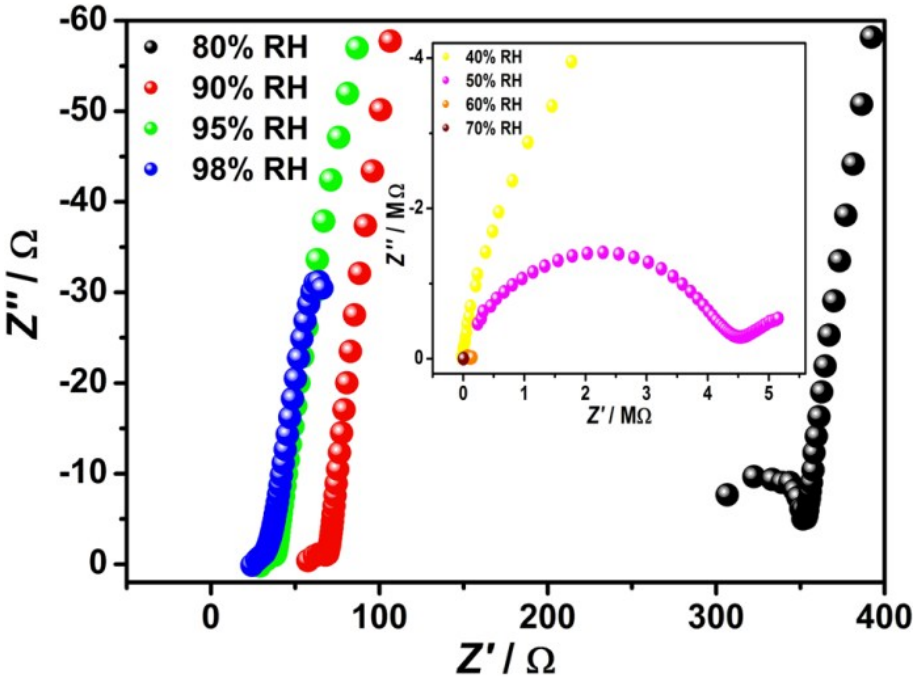

Figure S22. Nyquist plots from AC impedance data of IM-UiO-66-AS at 30 °C and different humidities variation from 40% to 98% RH.

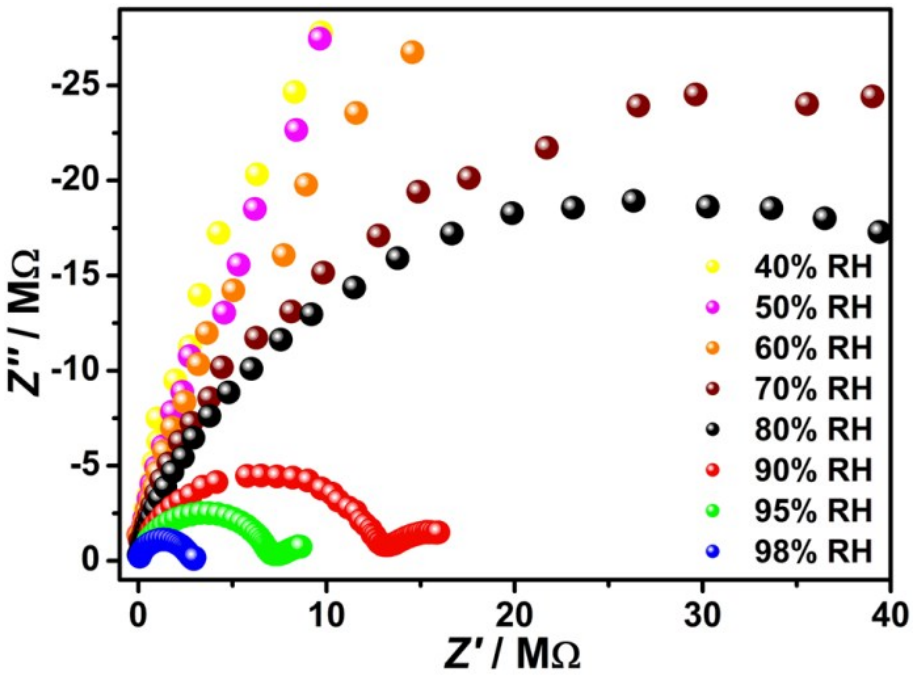

Figure S23. Nyquist plots from AC impedance data of UiO-66-NH_2 at 30 °C and different humidities variation from 40% to 98% RH.

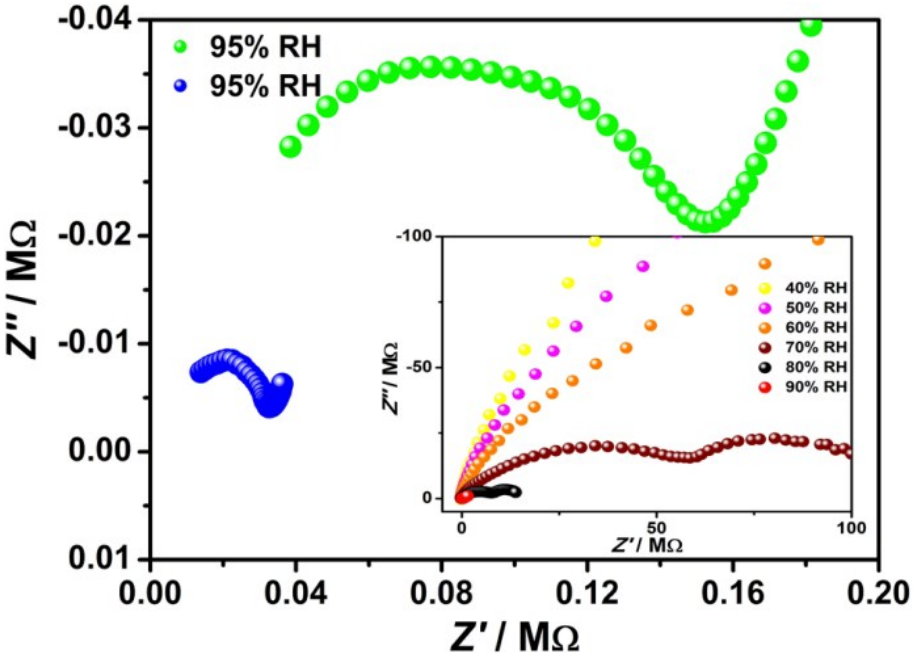

Figure S24. Nyquist plots from AC impedance data of UiO-66-AS at 30 °C and different humidities variation from 40% to 98% RH.

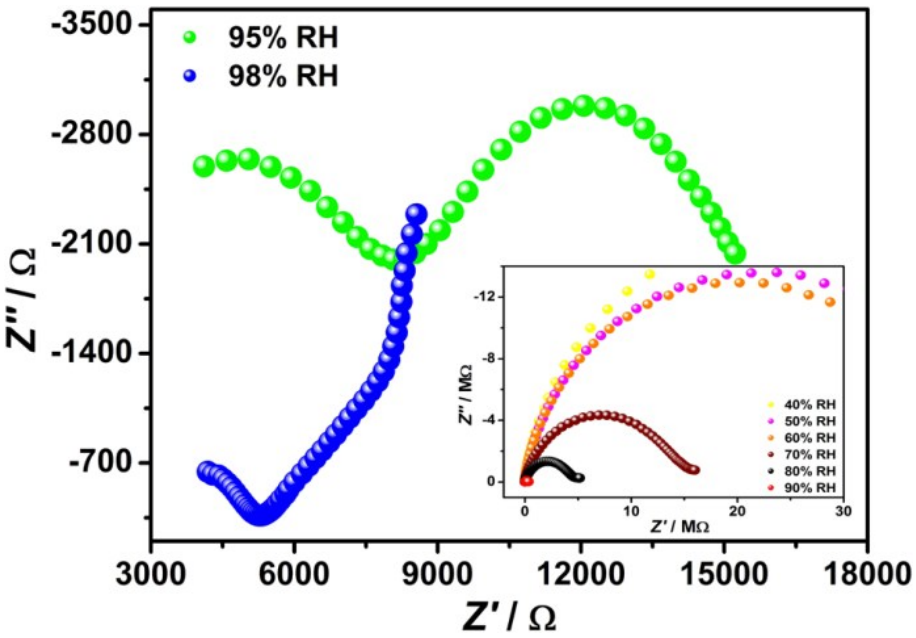

Figure S25. Nyquist plots from AC impedance data of UiO-66-SO_3H at 30 °C and different humidities variation from 40% to 98% RH.

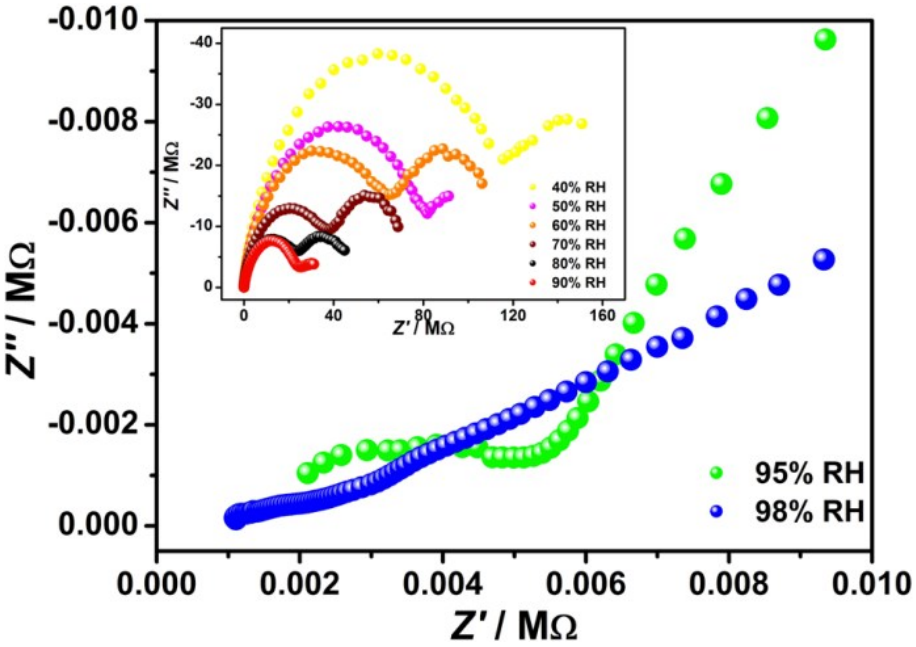

Figure S26. Nyquist plots from AC impedance data of UiO-66-NH_2-IM at 30 °C and different humidities variation from 40% to 98% RH.

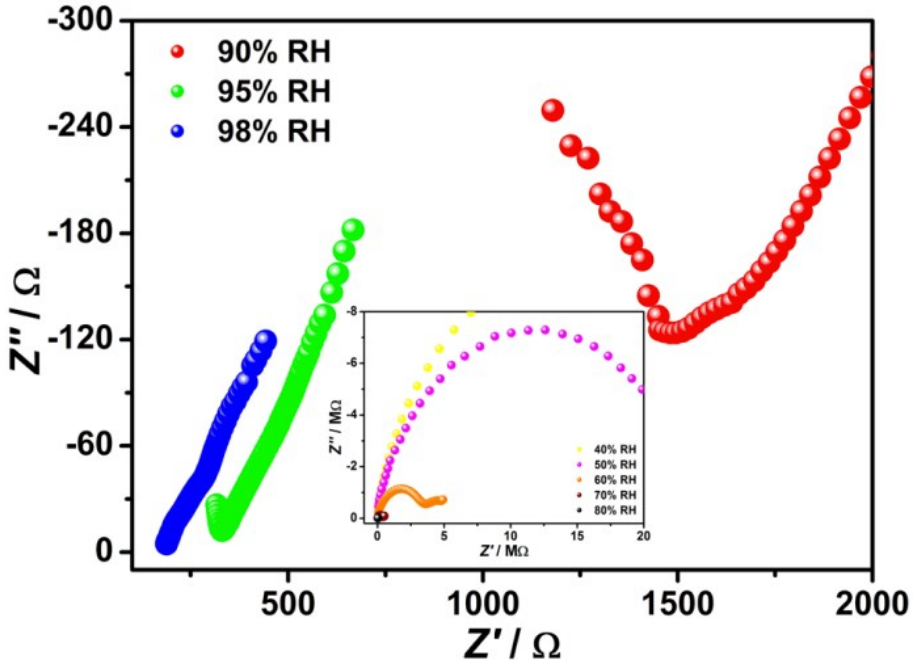

Figure S27. Nyquist plots from AC impedance data of UiO-66-AS without cleaning at 30 °C and different humidities variation from 40% to 98% RH.

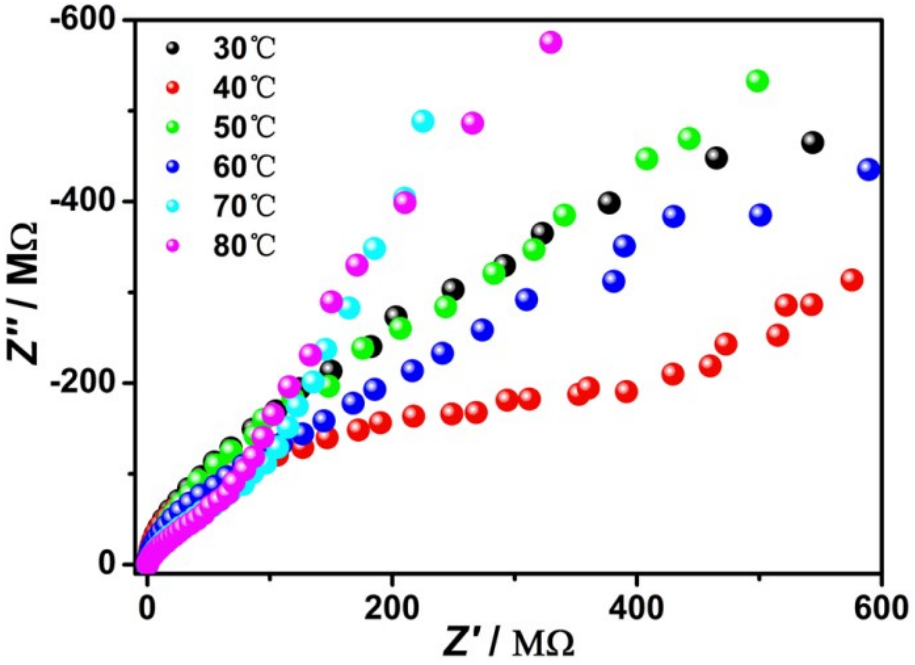

Figure S28. Nyquist plots from AC impedance data of UiO-66-NH_2 at 40% RH and different temperatures variation from 30 to 80 °C.

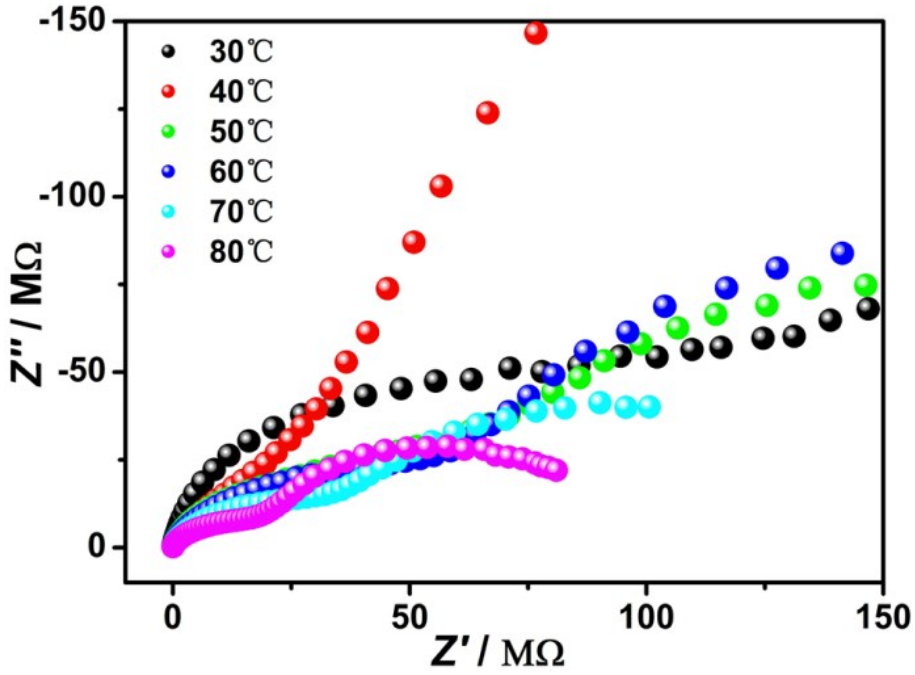

Figure S29. Nyquist plots from AC impedance data of UiO-66-AS at 40% RH and different temperatures variation from 30 to 80 °C.

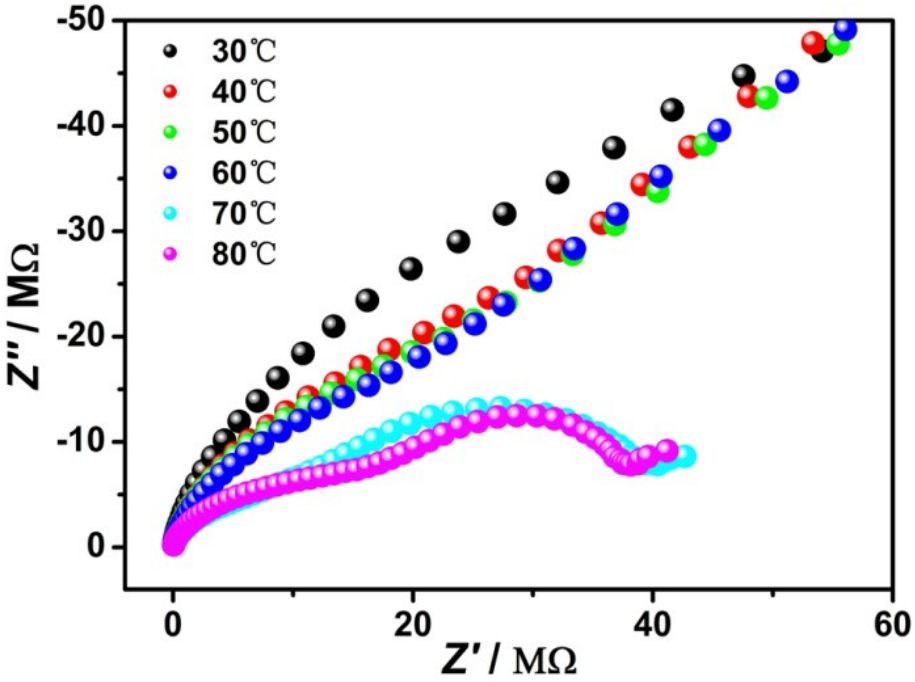

Figure S30. Nyquist plots from AC impedance data of IM-UiO-66-AS at 40% RH and different temperatures variation from 30 to 80 °C.

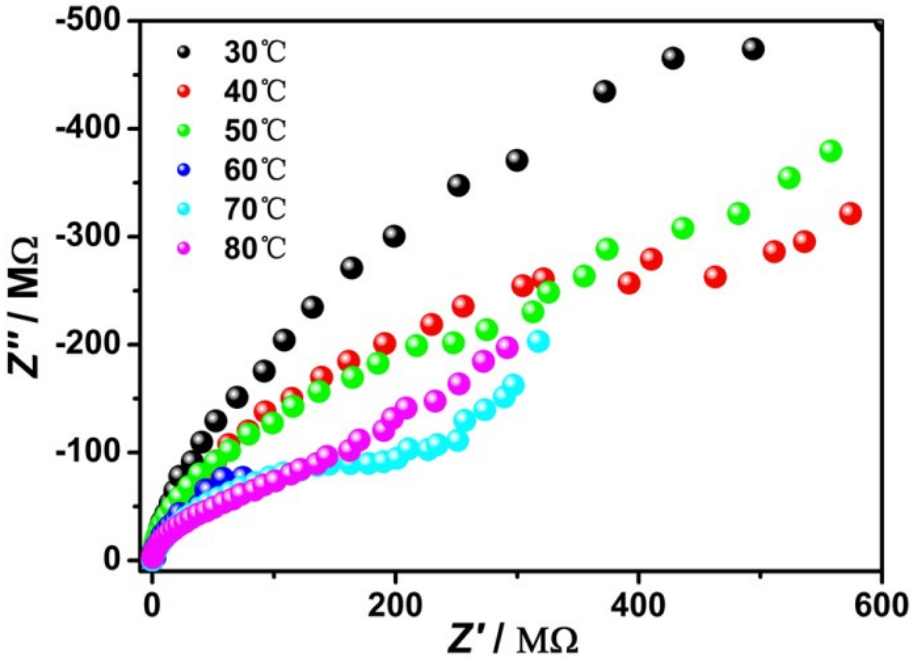

Figure S31. Nyquist plots from AC impedance data of UiO-66-SO_3H at 40% RH and different temperatures variation from 30 to 80 °C.

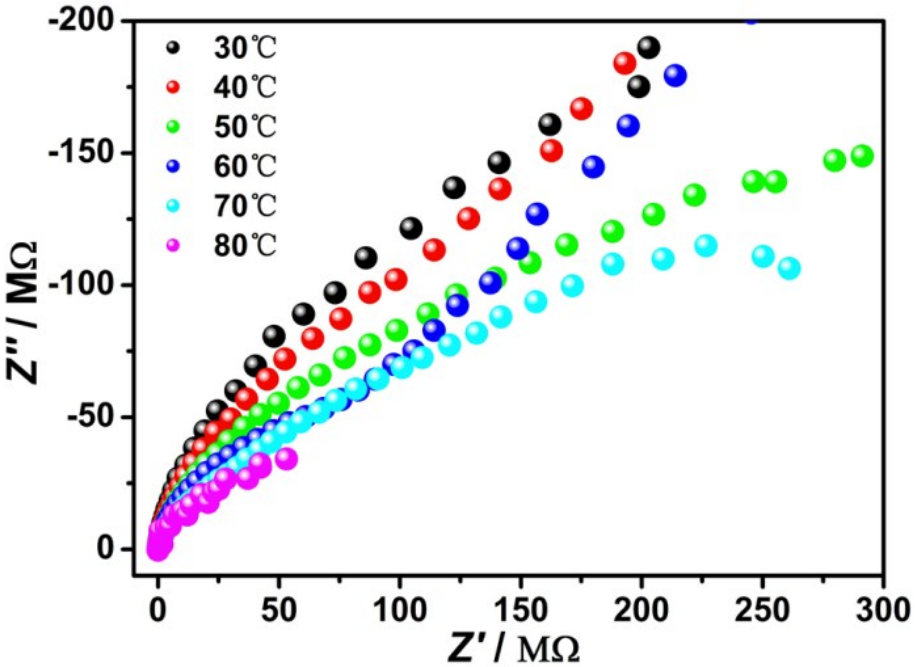

Figure S32. Nyquist plots from AC impedance data of UiO-66-NH_2-IM at 40% RH and different temperatures variation from 30 to 80 °C.

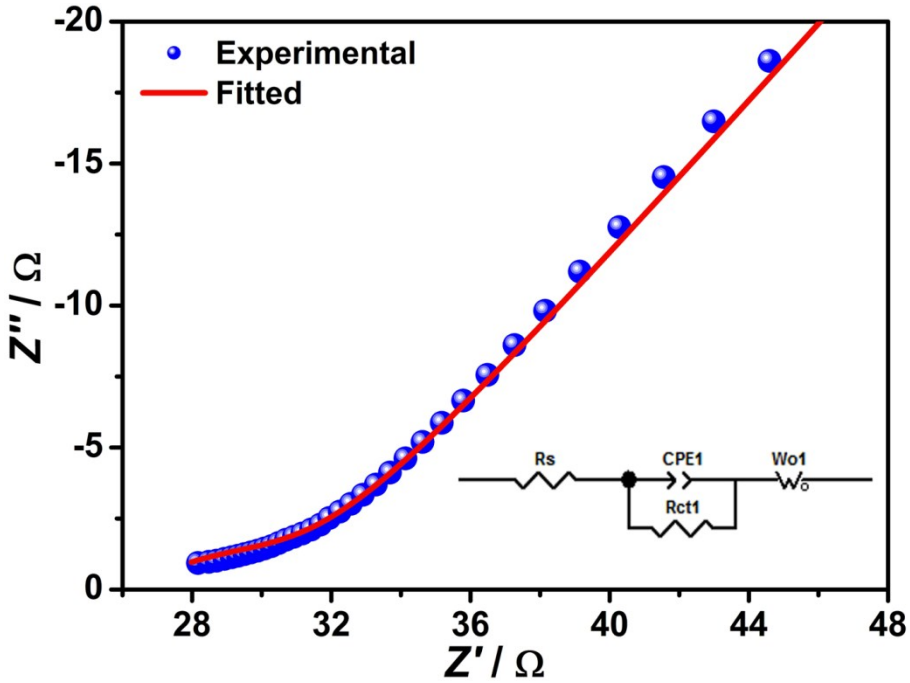

Figure S33. Fitting for the Nyquist plot at 80 °C and 98% RH of IM-UiO-66-AS, with circuit model used for the data fitting shown as an inset.

Table S4. The parameters for circuit model of IM-UiO-66-AS at 80 °C and 98% RH.

Element	Value
Rs	26.15
CPE1-T	0.00034815
CPE1-P	0.42663
Rct1	4.829
Wo1-R	3.086
Wo1-T	4.6504E-6
Wo1-P	0.30062

Table S5. Comparison of proton conductivity of IM-UiO-66-AS with some other representative MOFs-based proton conductors measured under hydrous condition.

Compounds	**Conditions**	**σ (S cm^{-1})**	**E_a**	**Reference**

			(eV)	
IM-UiO-66-AS (bulk conductivity)	80 °C, 98% RH	1.54×10^{-1}	0.20	This work
Nafion	30 °C, 98% RH	5×10^{-2}	0.22	4
$Fe(ox)\cdot2H_2O$	45 °C, 98% RH	3.23×10^{-3}	0.37	5
PCMOF-3	25 °C, 98% RH	3.5×10^{-5}	0.17	6
$(NH_4)_4[MnCr_2(ox)_6]\cdot4H_2O$	40 °C, 96% RH	1.7×10^{-3}	0.23	7
$Fe(OH)(bdc\text{-}(COOH)_2)$	80 °C, 95% RH	7×10^{-6}	0.21	8
$Cu_3Mo_5P_2$	28 °C, 98% RH	2.2×10^{-5}	0.232	9
$\{NMe_3(CH_2COOH)\}[FeCr(ox)_3]\cdot nH_2O$	25 °C, 65% RH	0.8×10^{-4}	/	10
$\{NEt_3(CH_2COOH)\}[MnCr(ox)_3]\cdot nH_2O$	25 °C, 80% RH	2×10^{-4}	/	10
$\{NBu_3(CH_2COOH)\}[MnCr(ox)_3]\cdot nH_2O$	25 °C, 90% RH	5×10^{-6}	/	10
$\{NBu_3(CH_2COOH)\}[FeCr(ox)_3]\cdot nH_2O$	25 °C, 90% RH	0.9×10^{-7}	/	10
Ca-SBBA	25 °C, 98% RH	8.58×10^{-6}	0.23	11
Sr-SBBA	25 °C, 98% RH	4.4×10^{-5}	0.56	11
In-IA-2D-1	27 °C, 98% RH	3.4×10^{-3}	0.61	12
In-IA-2D-2	27 °C, 98% RH	4.2×10^{-4}	0.48	12
PCMOF-5	60 °C, 98% RH	2.51×10^{-3}	0.16	13
$\{H[Cu(Hbpdc(H_2O)_2]_2[PMo_{12}O_{40}]\cdot nH_2O\}_n$	100 °C, 98% RH	1.25×10^{-3}	1.02	14
$\{H[Cu(Hbpdc(H_2O)_2]_2[PW_{12}O_{40}]\cdot nH_2O\}_n$	100 °C, 98% RH	156×10^{-3}	1.02	14
$\{[Ca(D\text{-}Hpmpc)(H_2O)_2]\cdot2HO_{0.5}\}_n$	60 °C, 97% RH	8.9×10^{-4}	0.21	15
$\{H[Ni(Hbpdc)(H_2O)_2]_2[PW_{12}O_{40}]\cdot8H_2O$	100 °C, 98% RH	1.35×10^{-3}	1.01	16
$\{[H_3O][Cu_2(DSOA)(OH)(H_2O)]\cdot9.5H_2O\}_n$	85 °C, 98% RH	1.9×10^{-3}	1.04	17
PCMOF2½	85 °C, 90% RH	2.1×10^{-2}	0.21	18
$\{[(Me_2NH_2)_3(SO_4)]_2[Zn(ox)_3]\}_n$	25 °C, 98% RH	4.2×10^{-2}	0.129	19

EuL	75 °C, 97% RH	1.6×10^{-5}	0.91	20
DyL	75 °C, 97% RH	1.33×10^{-5}	0.87	20
HKUST-1	90 °C, 70% RH	1.08×10^{-8}	0.69	21
NENU-3	90 °C, 70% RH	4.76×10^{-5}	0.41	21
NENU-3-Ina	90 °C, 70% RH	1.81×10^{-3}	0.36	21
$(NH_4)_2(adp)[Zn_2(ox)_3]\cdot2H_2O$	25 °C, 100% RH	7×10^{-5}	/	22
$(NH_4)_2(adp)[Zn_2(ox)_3]\cdot3H_2O$	25 °C, 100% RH	8×10^{-3}	/	22
$H^+@Ni_2(dobdc)$ pH=1.8	80 °C, 95% RH	2.2×10^{-2}	0.12	23
$\{[Cu_3(L)_2(H_2O)_4][Cu(dmf)_4(SiW_{12}O_{40})]\cdot9H_2O$	100 °C, 98% RH	5.94×10^{-4}	0.32	24
$[H_3O][CoLa(notp)(H_2O)_4]ClO_4\cdot3H_2O$	25 °C, 98% RH	4.24×10^{-5}	0.28	25
$[Cu_3(u_3OH)(H_2O)_3(atz)_3]_3[P_2W_{18}O_{62}]\cdot14H_2O$	25 °C, 97% RH	4.4×10^{-6}	/	26
$[Cu(H_2L)(DMF)_4]_n$	95 °C, 95% RH	3.46×10^{-3}	0.68	27
$[CaL_{0.5}(DMF)_{2.5}]_n$	25 °C, 95% RH	1.27×10^{-5}	0.17	27
$[CdL_{0.5}(DMF)_2]_n$	25 °C, 95% RH	2.49×10^{-7}	0.59	27
$[Cd_2(btc)_2(H_2O)_2]_n\cdot n(H_2bmib)\cdot6n(H_2O)$	60 °C, 95% RH	5.4×10^{-5}	0.62	28
$[Cd_4(cpip)_2(Hcpip)_2]_n\cdot n(H_2bmib)\cdot n(H_2O)$	60 °C, 95% RH	2.2×10^{-5}	0.27	28
ZIF8	94 °C, 98% RH	4.6×10^{-4}	/	29
PCMOF10	70 °C, 95% RH	3.55×10^{-2}	0.4	30
$\{[Zn(C_{10}H_2O_8)_{0.5}(C_{10}S_2N_2H_8)]\cdot5H_2O]\}_n$	80 °C, 95% RH	2.55×10^{-7}	0.96	31
$\{[Zn(C_{10}H_2O_8)_{0.5}(C_{10}S_2N_2H_8)]\cdot2H_2O]\}_n$	80 °C,95% RH	4.39×10^{-4}	0.84	31
$Cu_4(L)_2(OH)_2(DMF)_2$	95 °C, 95% RH	7.4×10^{-4}	1.32	32
$UiO\text{-}66(SO_3H)_2$	80 °C, 90% RH	8.4×10^{-2}	0.32	33
$UiO\text{-}66(Zr)\text{-}(CO_2H)_2$	90 °C, 95% RH	2.3×10^{-3}	0.17	34
$[Cu_3(BTC)_2(H_2O)_3]_4[SiW_{11}Mo^{V}O_{40}](C_4H_{12}N_5)\cdot30H_2O$	25 °C, 97% RH	6.37×10^{-8}	/	35

VNU-15	95 °C, 60% RH	2.90×10^{-2}	0.22	36
MFM-500 (Ni)	25 °C, 98% RH	4.5×10^{-4}	0.43	37
H_2SO_4@MIL-101 (3M)	70 °C, 90% RH	6.87×10^{-1}	0.30	38
H_2SO_4@MIL-101-SO_3H (3M)	70 °C, 90% RH	1.82	0.47	38
BUT-8-(Cr)A	80 °C, 100% RH	1.27×10^{-1}	0.11	39
Im@Fe-MOF	60 °C, 98% RH	1.21×10^{-2}	0.436	40
PCMOF-17	25 °C, 40% RH	1.17×10^{-3}	0.31	41
(Me_2NH_2)[Eu(L)]	100 °C, 98% RH	3.76×10^{-3}	0.38	42
JLU-Liu44	27 °C, 98% RH	8.4×10^{-3}	0.25	43
TETA@3	80 °C, 100% RH	1.52×10^{-2}	0.22	44
$(N_2H_5)[CeEu(C_2O_4)_4(N_2O_5)]$ •$4H_2O$	25 °C, 100% RH	3.42×10^{-3}	0.1	45
Im@(NENU-3)	70 °C, 90% RH	1.82×10^{-2}	0.57	46
La-PCMOF-5	85 °C, 95% RH	6×10^{-3}	0.17	47
Ce-PCMOF-5	85 °C, 95% RH	1.2×10^{-4}	0.2	47
Pr-PCMOF-5	85 °C, 95% RH	3.9×10^{-3}	0.17	47
Nd-PCMOF-5	85 °C, 95% RH	2.1×10^{-4}	0.24	47
Sm-PCMOF-5	85 °C, 95% RH	2.3×10^{-4}	0.24	47
Eu-PCMOF-5	85 °C, 95% RH	1.9×10^{-4}	0.23	47
Gd-PCMOF-5	85 °C, 95% RH	1.5×10^{-4}	0.19	47
Ni-BDP-COOH	80 °C, 97% RH	2.22×10^{-3}	0.11	48
PCMOF2½(Pz)	85 °C, 90% RH	1.1×10^{-1}	0.16	49
1⊃pz·6HCl	80 °C, 95% RH	2.94×10^{-2}	0.38	50
MIP-202(Zr)	90 °C, 95% RH	1.1×10^{-2}	0.22	51
MFM-555(Ho)	20 °C, 99% RH	2.51×10^{-4}	0.32	52
KAUST-7'	90 °C, 95% RH	2×10^{-2}	0.19	53
MIT-25	75 °C, 95% RH	5.1×10^{-4}	0.40	54
$[Cu(p\text{-}IPhHIDC)]_n$	100 °C, 98% RH	1.51×10^{-3}	0.25	55
SmHEDP-TEG	60 °C, 100% RH	9.17×10^{-2}	0.49	56
$\{(H_3O)[Tb(BoDSDC)(H_2O)_2]\}_n$	85 °C, 95% RH	6.57×10^{-4}	0.541	57

Im = Imidazole, ox = oxalate, PCMOF-3 = $Zn_3(L)(H_2O)_2\cdot2H_2O$ (L = 1,3,5-benzenetriphosphonate), H_2bdc = 1,4-benzenedicarboxylic acid, In-IA-2D-1 = $[In(IA)_2\{(CH_3)_2NH_2\}(H_2O)_2]$ In-IA-2D-2 = $[In(IA)_2\{(CH_3)_2NH_2\}(DMF)]$ (IA = isophthalic acid), PCMOF-5 = $LaH_5L(H_2O)_4$ (L = Benzene-1,2,4,5-

tetramethylenephosphonic acid), H_2bpd = 2,2′-bipyridyl-3,3′-dicarboxylic acid, D-H_2pmpc = D-1-(phosphonomethyl)piperdine-3-carboxylic acid, Na_2H_2DSOA = disodium-2,2′-disulfonate-4,4′-oxydibenzoic acid, adp = adipic acid, dobdc^{4-} = 2,5-dioxido-1,4-benzenedicarboxylate, notpH_6=$C_9H_{18}N_3(PO_3H_2)_3$, Hatz = 3-amino-1,2,4,triazolate, H_3btc = 1,3,5-benzenetricarboxylic acid, H_3cpip = 5-(4-carboxyphenoxy)isophthalic acid, PCMOF10 = $Mg_2(H_2O)_4(H_2L)\cdot H_2O$ (H_6L = 2,5-dicarboxy-1,4-benzenediphosphonic acid), BTC = 1,3,5-benzenetricarboxylate, VNU-15 = $Fe_4(BDC)_2(NDC)(SO_4)_4(DMA)_4$ (BDC = benzene-1,4-dicarboxylate, NDC = naphthalene-2,6-dicarboxylate), MFM-500(Ni) = $[M_3(H_3L)_2(H_2O)_9(C_2H_6SO)_3]$ (M=Ni, H_6L = benzene-1,3,5-p-phenylphosphonic acid), (Me_2NH_2)[Eu(L)] H_4L=5-(phosphonomethyl) isophthalic acid, H_2BDP=1,4-bis(4-pyrazoly)benzene, p-IphH$_3$IDC=2-(p-N-imidazol-1-yl)-phenyl-1H-imidazole-4,5-dicarboxylic acid, H_4-BODSDC=benzophenone-3,3'-disulfonyl-4,4'-dicarboxylic acid.

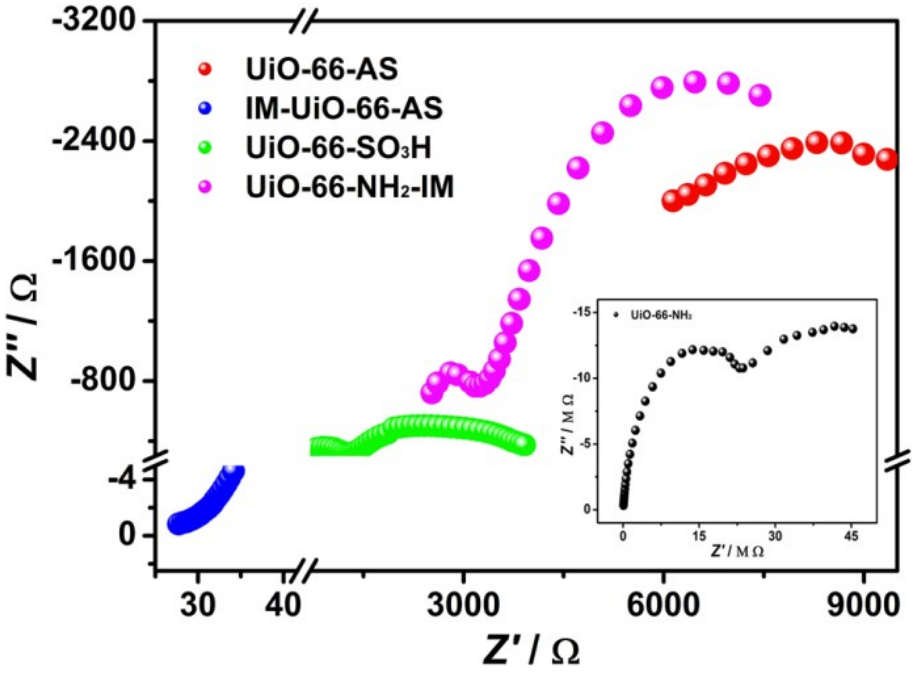

Figure S34. Nyquist plots from AC impedance data of UiO-66-NH_2 (insert, black), UiO-66-AS (red), IM-UiO-66-AS (blue), UiO-66-SO_3H (green) and UiO-66-NH_2-IM (magenta) at 80 °C and 98% RH.

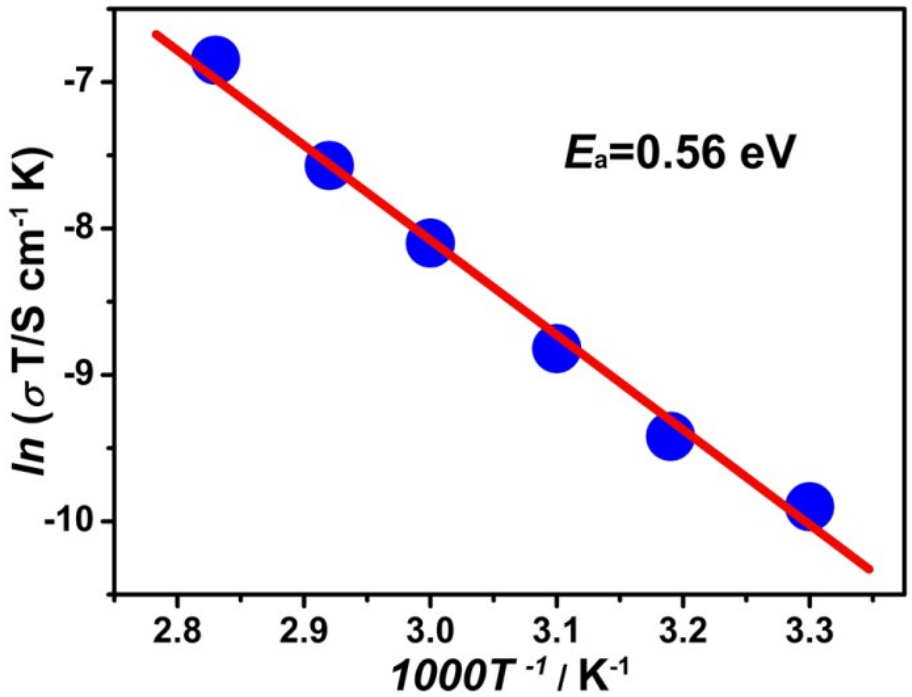

Figure S35. Arrhenius plot of UiO-66-NH_2 (at the temperature range of 30-80 °C and 98% RH).

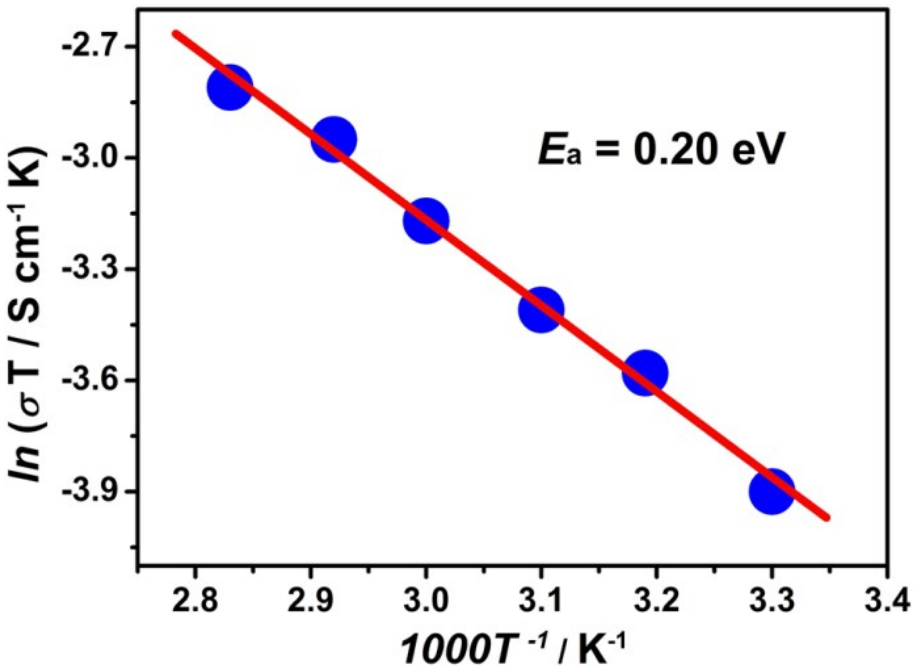

Figure S36. Arrhenius plot of UiO-66-AS (at the temperature range of 30-80 °C and 98% RH).

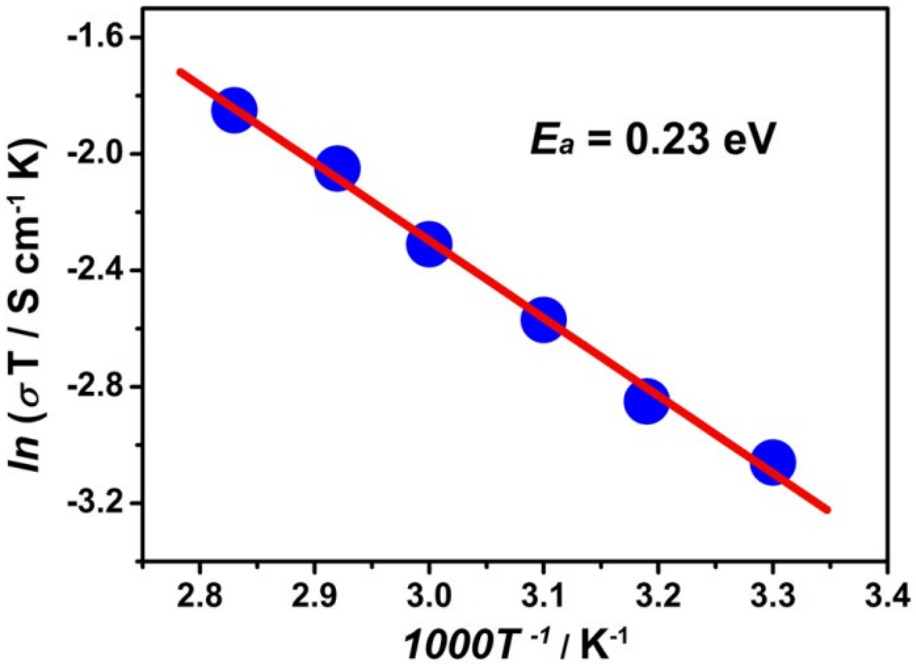

Figure S37. Arrhenius plot of UiO-66-SO_3H (at the temperature range of 30-80 °C and 98% RH).

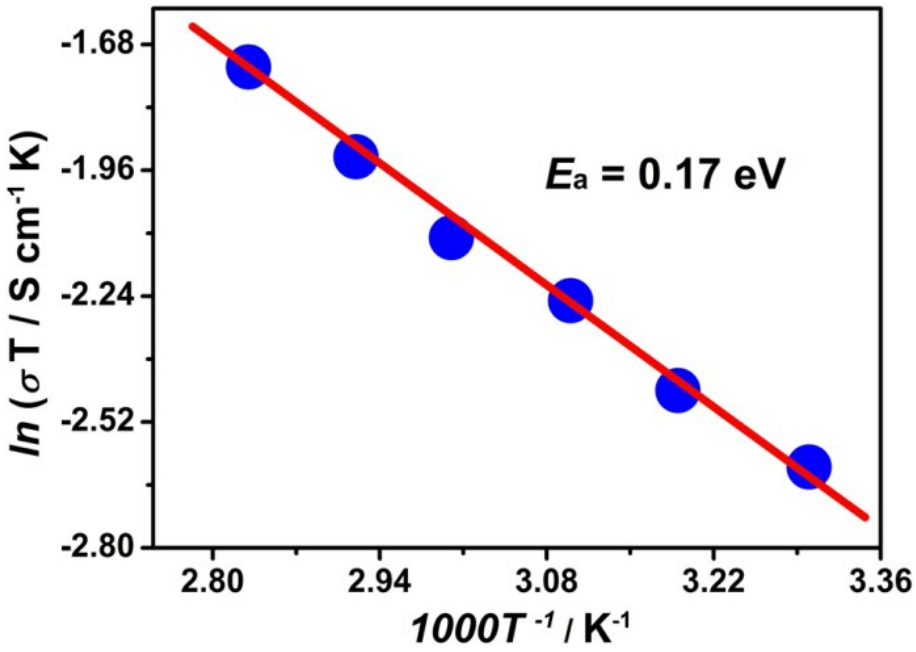

Figure S38. Arrhenius plot of UiO-66-NH_2-IM (at the temperature range of 30-80 °C and 98% RH).

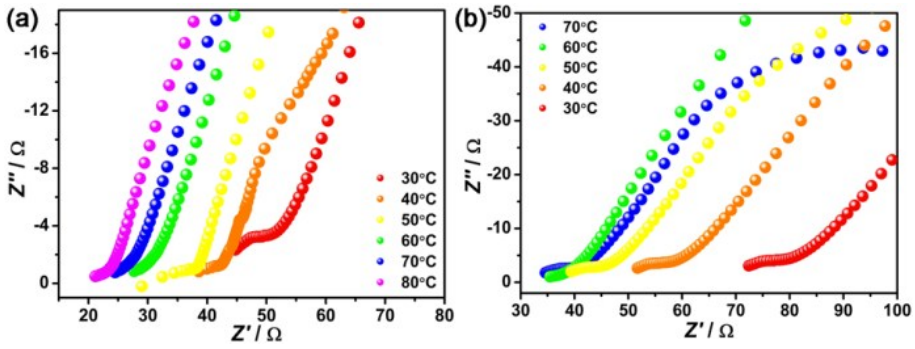

Figure S39. Nyquist plots from AC impedance data for the heating-cooling cycles of IM-UiO-66-AS under 98% RH. (a) the first heating cycle (30-80 °C), (b) the first cooling cycle (70-30 °C).

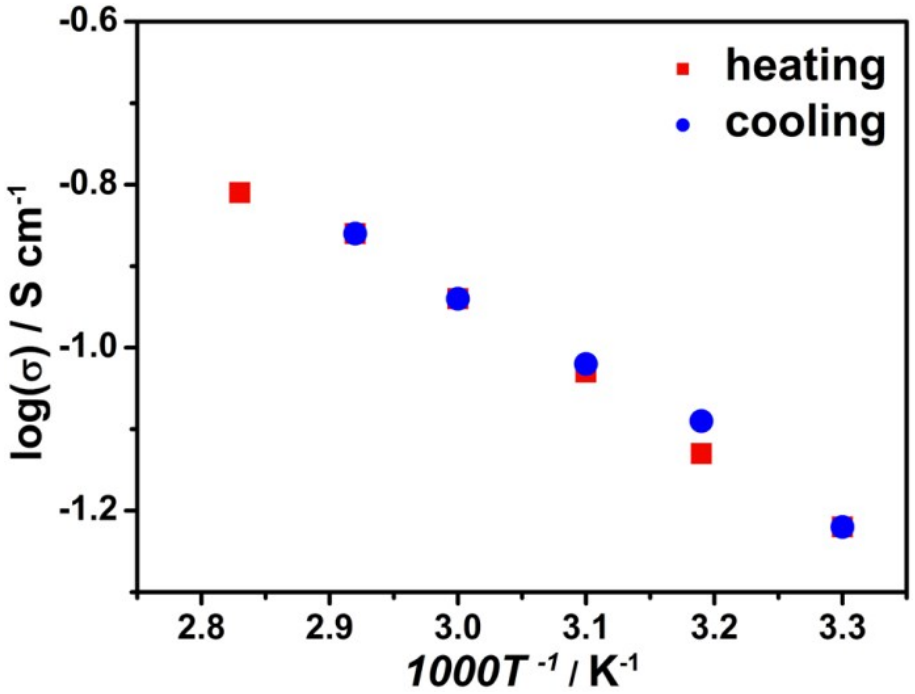

Figure S40. Log-scaled proton conductivities for the heating-cooling cycles of IM-UiO-66-AS at 98% RH.

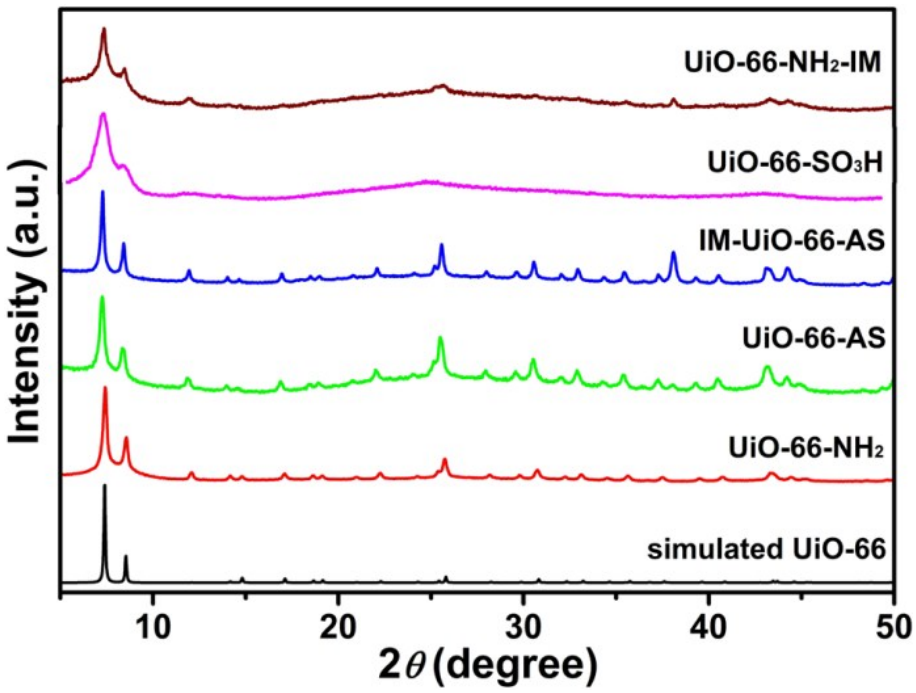

Figure S41. PXRD patterns of simulated UiO-66 (black) and UiO-66-NH_2 (red), UiO-66-AS (green), IM-UiO-66-AS (blue), UiO-66-SO_3H (magenta) and UiO-66-NH_2-IM (wine) undergoing proton conduction measurements.

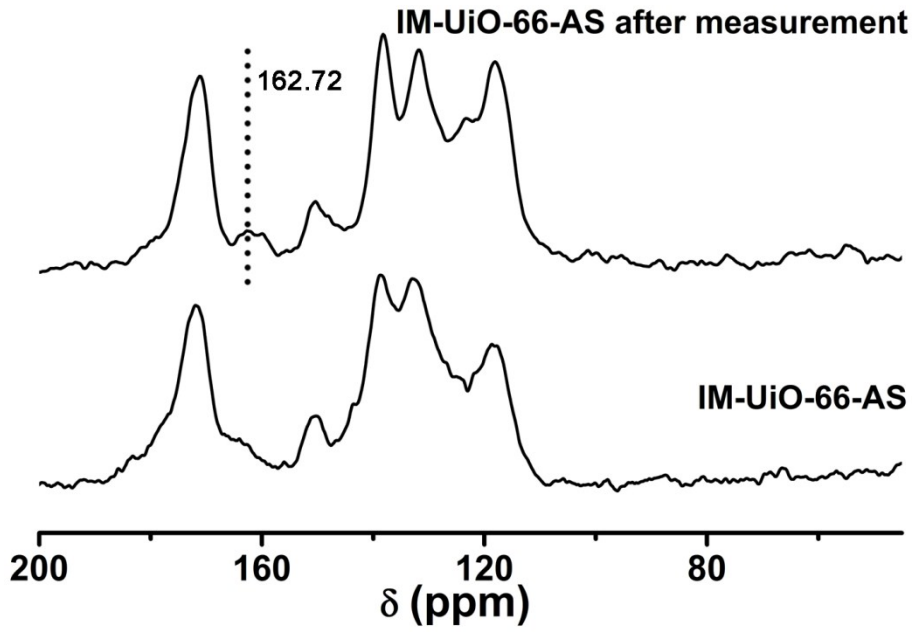

Figure S42. Solid state ^{13}C CP/MAS NMR spectrum of IM-UiO-66-AS undergoing proton conduction measurement.

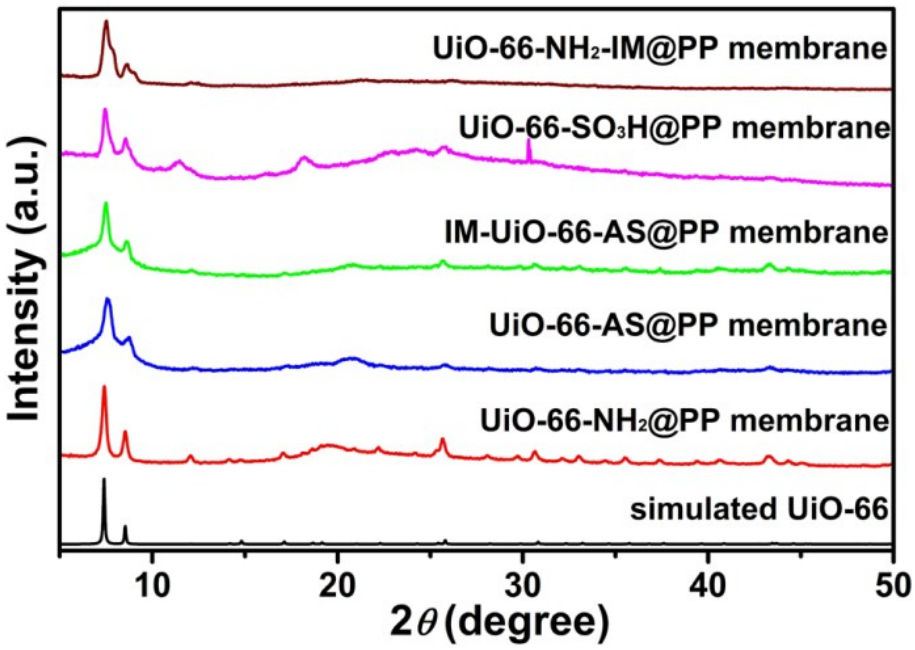

Figure S43. PXRD patterns of simulated UiO-66 (black), as-synthesized UiO-66-NH_2@PP membrane (red), as-synthesized UiO-66-AS@PP membrane (blue), as-synthesized IM-UiO-66-AS@PP membrane (green), as-synthesized UiO-66-SO_3H@PP membrane (magenta) and as-synthesized UiO-66-NH_2-IM@PP membrane (wine).

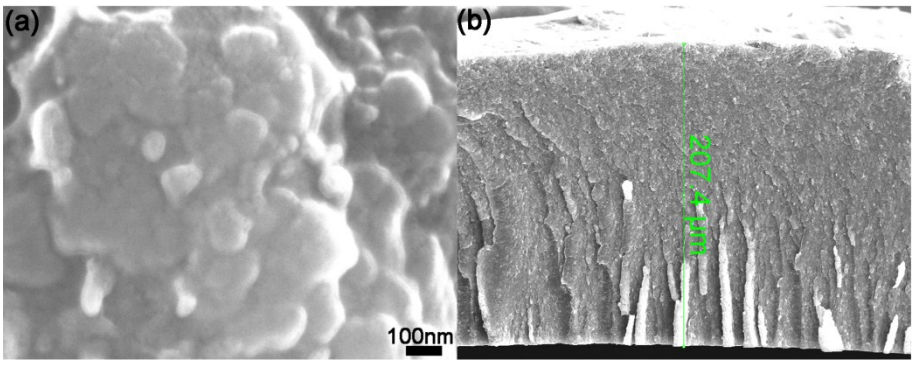

Figure S44. SEM images of as-synthesized UiO-66-NH_2@PP membrane: (a) the morphology, (b) the thickness.

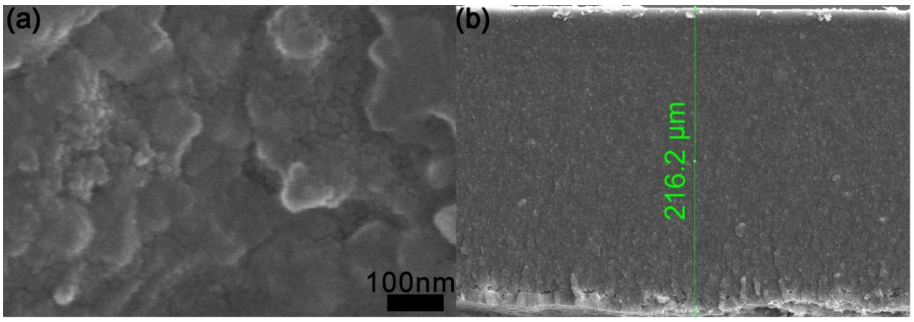

Figure S45. SEM images of as-synthesized UiO-66-AS@PP membrane: (a) the morphology, (b) the thickness.

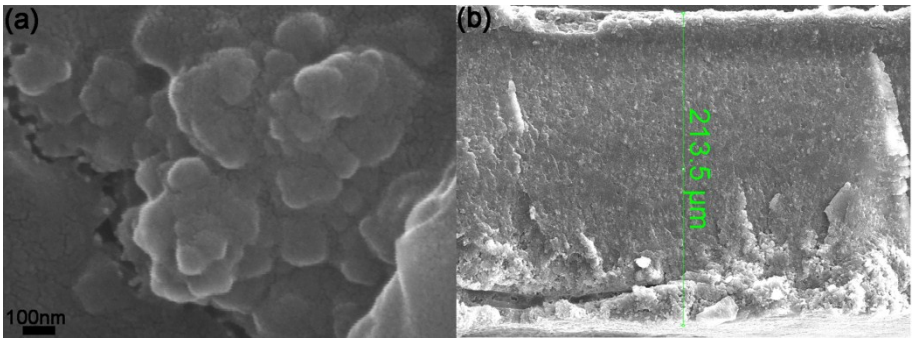

Figure S46. SEM images of as-synthesized IM-UiO-66-AS@PP membrane: (a) the morphology, (b) the thickness.

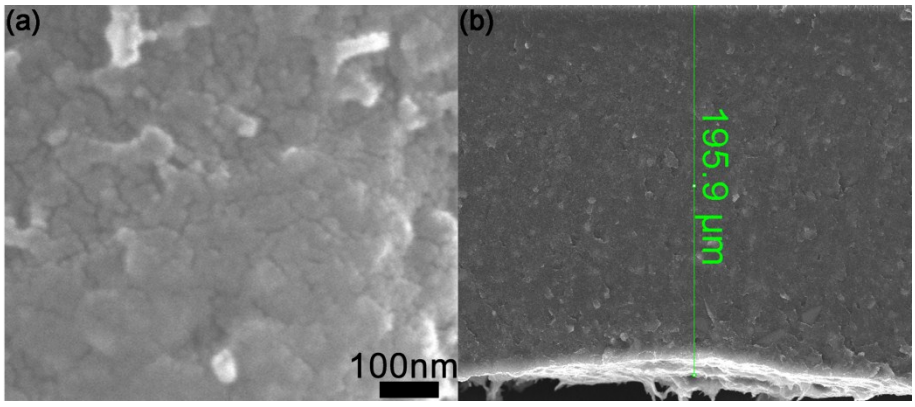

Figure S47. SEM images of as-synthesized UiO-66-SO_3H@PP membrane: (a) the morphology, (b) the thickness.

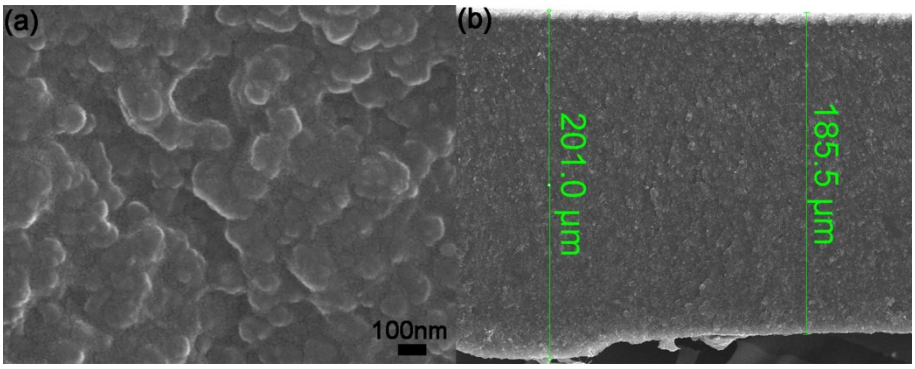

Figure S48. SEM images of as-synthesized UiO-66-NH_2-IM@PP membrane: (a) the morphology, (b) the thickness.

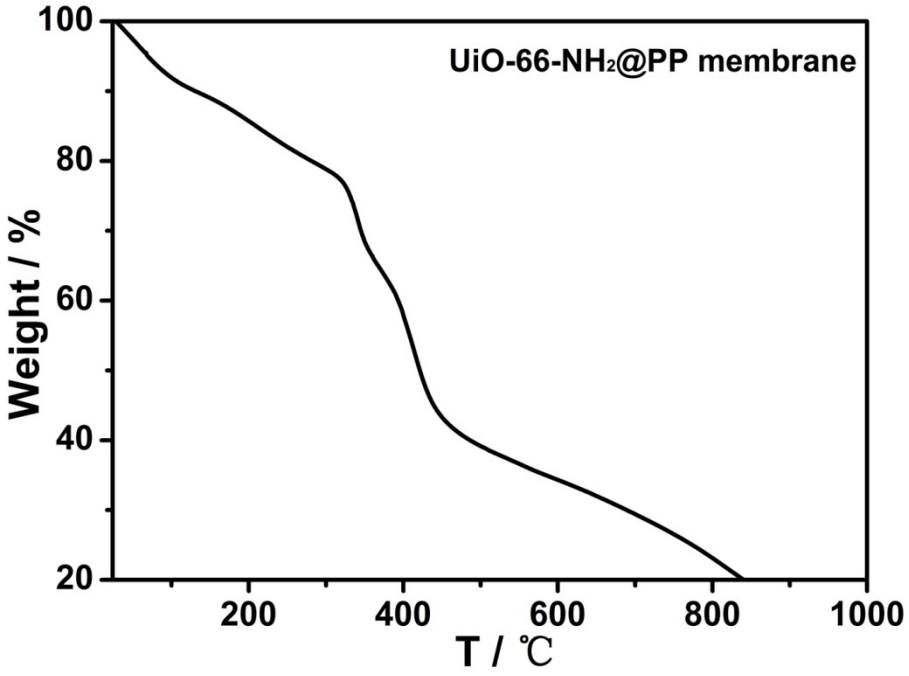

Figure S49. TGA traces of as-synthesized UiO-66-NH_2@PP membrane.

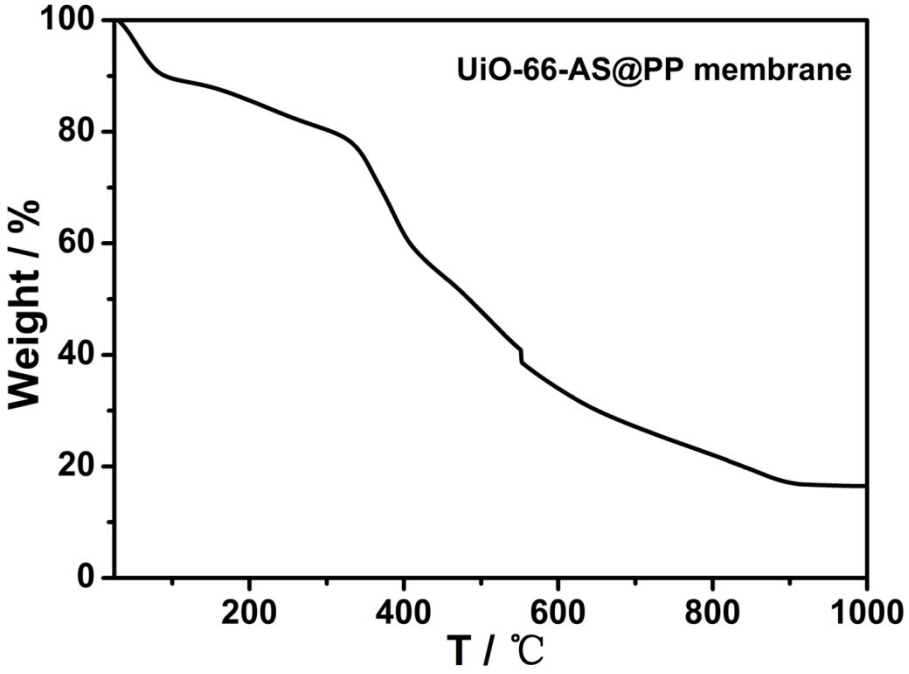

Figure S50. TGA traces of as-synthesized UiO-66-AS@PP membrane.

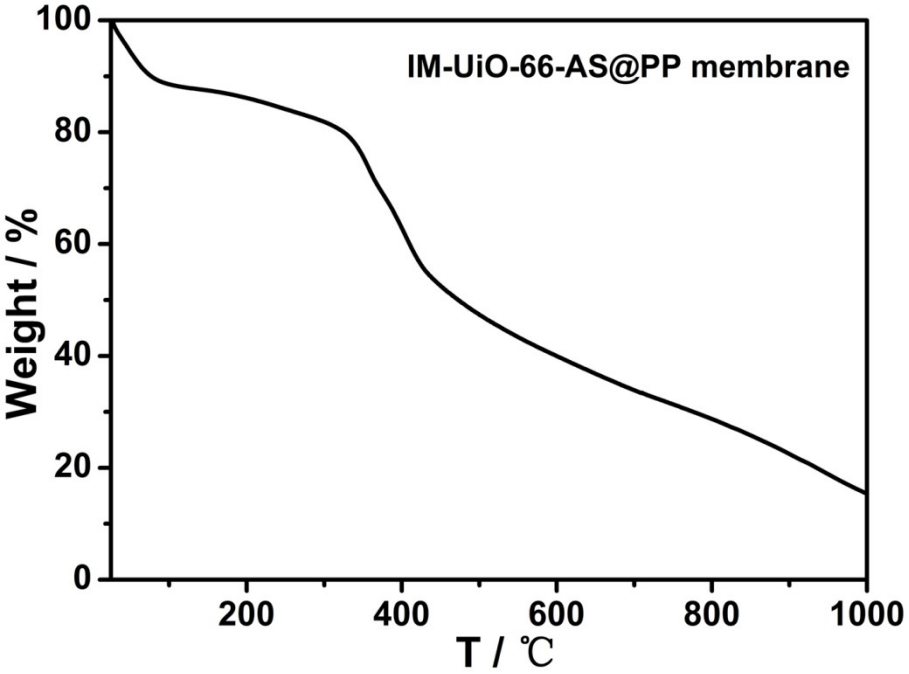

Figure S51. TGA traces of as-synthesized IM-UiO-66-AS@PP membrane.

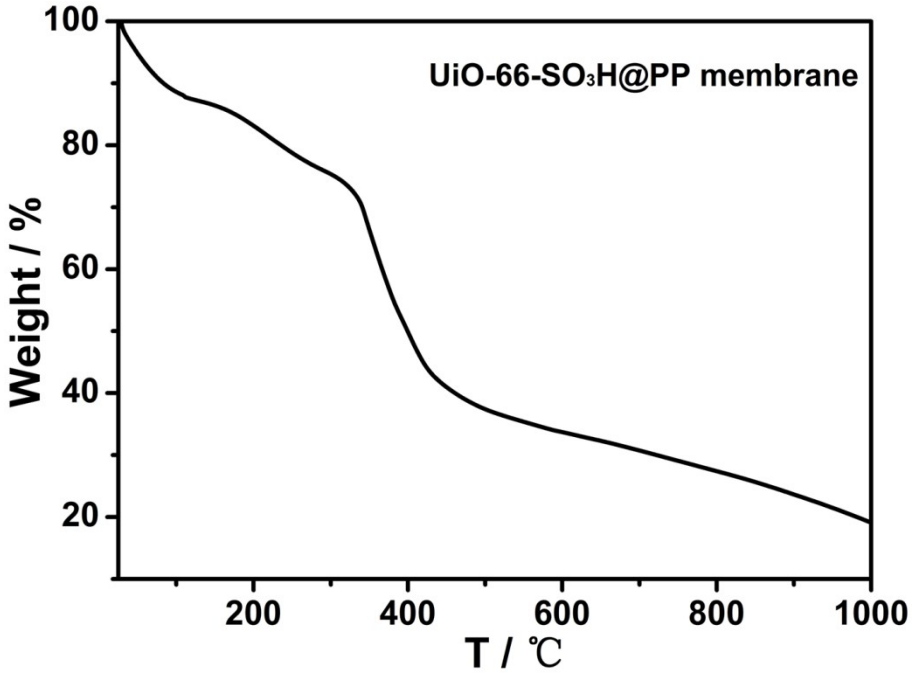

Figure S52. TGA traces of as-synthesized UiO-66-SO_3H@PP membrane.

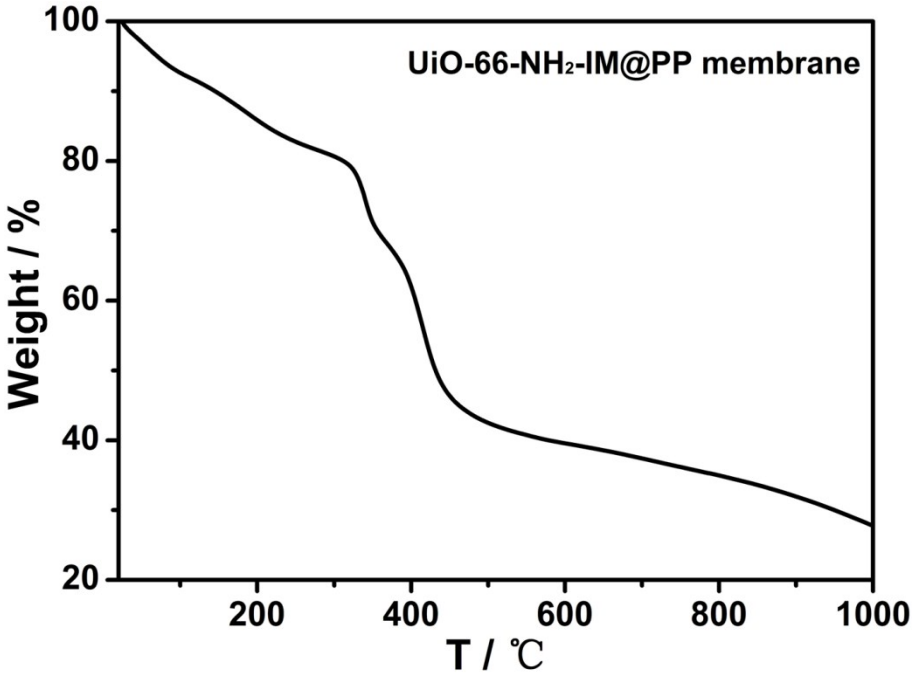

Figure S53. TGA traces of as-synthesized UiO-66-NH_2-IM@PP membrane.

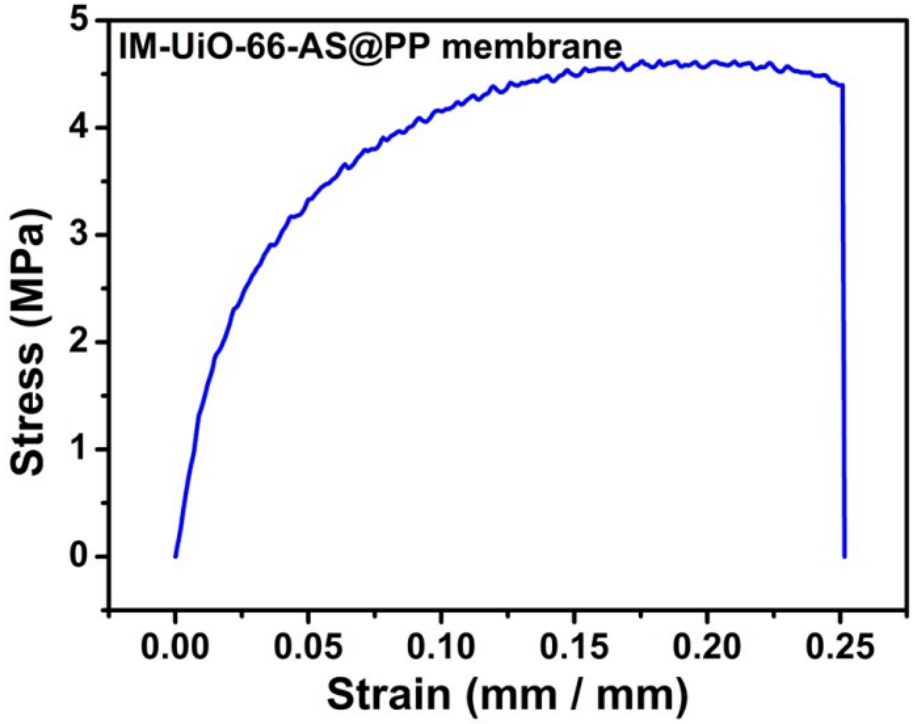

Figure S54. The stress-strain curve of IM-UiO-66-AS@PP membrane.

Table S6. Results of the Elastic Modulus, Ultimate tensile strength for IM-UiO-66-AS@PP membrane.

Material	Elastic Modulus (MPa)	Ultimate tensile strength (MPa)
IM-UiO-66-AS@PP membrane	152.98	4.62

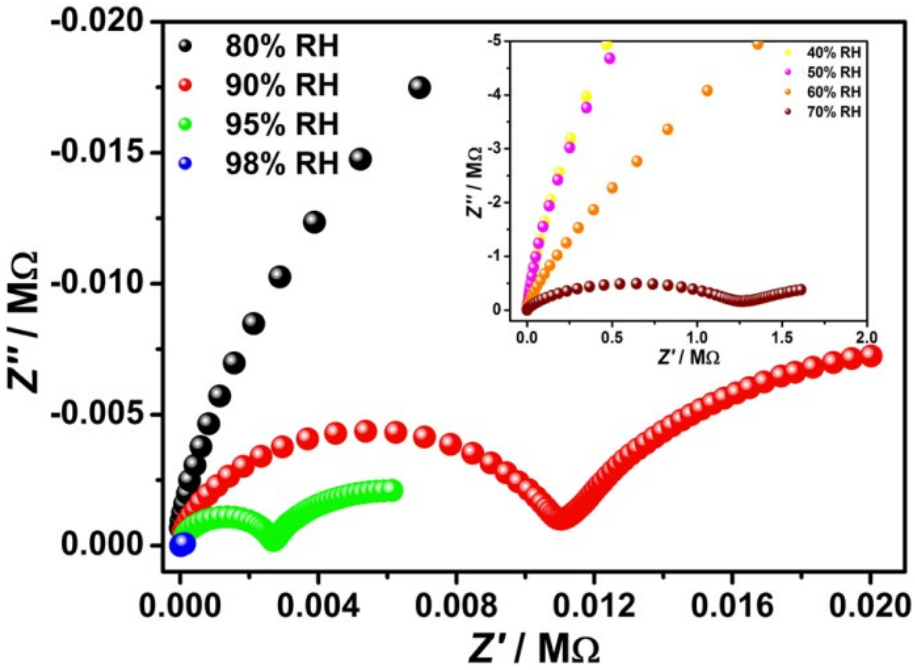

Figure S55. Nyquist plots from AC impedance data of IM-UiO-66-AS@PP membrane at 30 °C and different humidities variation from 40% to 98% RH.

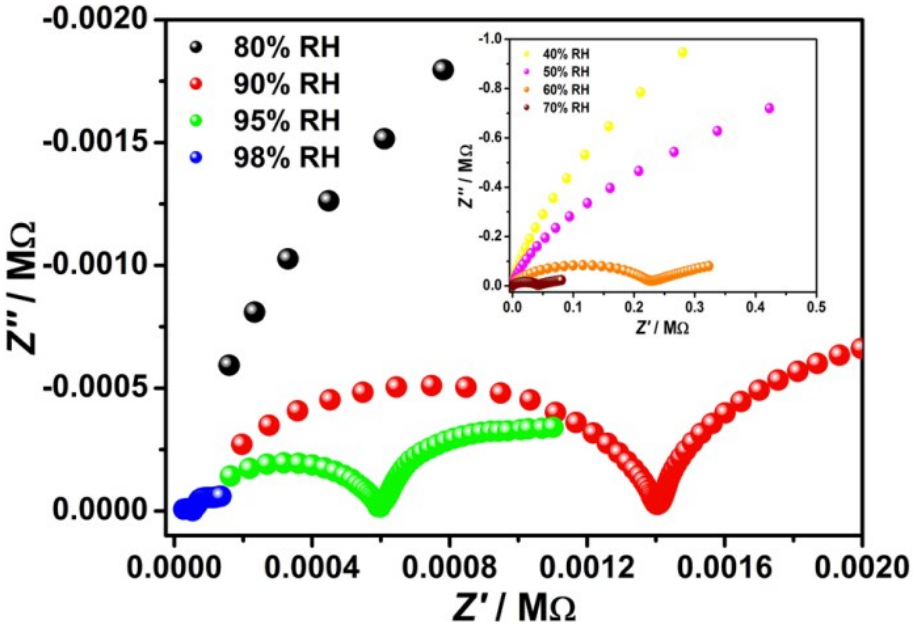

Figure S56. Nyquist plots from AC impedance data of UiO-66-NH_2@PP membrane at 30 °C and different humidities variation from 40% to 98% RH.

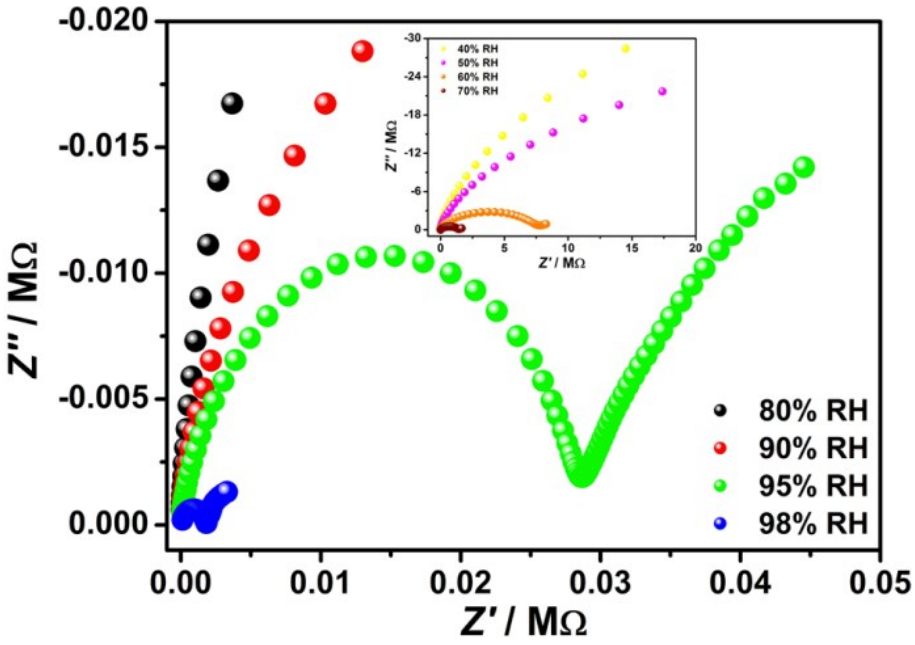

Figure S57. Nyquist plots from AC impedance data of UiO-66-AS@PP membrane at 30 °C and different humidities variation from 40% to 98% RH.

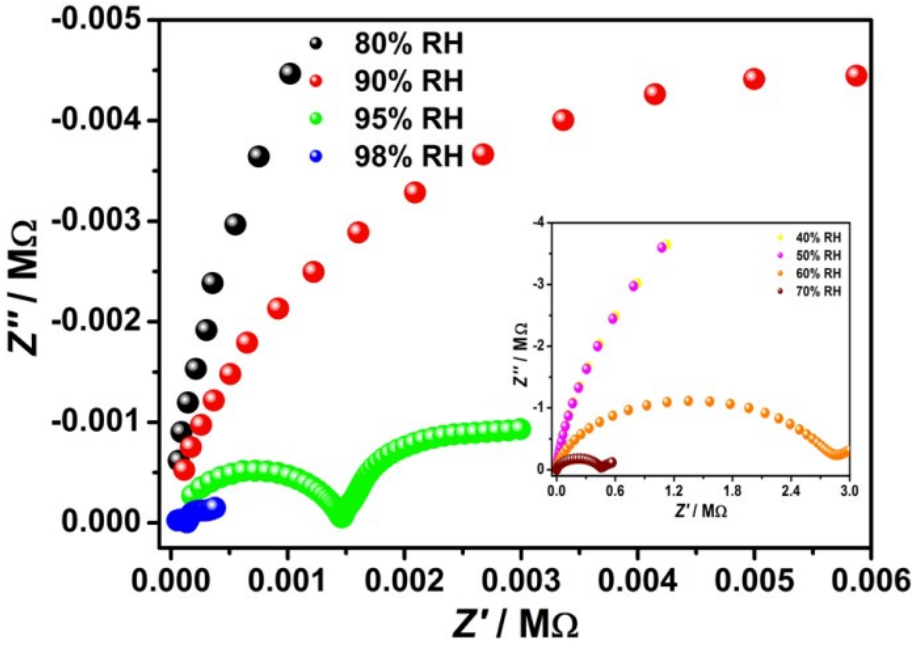

Figure S58. Nyquist plots from AC impedance data of UiO-66-SO_3H@PP membrane at 30 °C and different humidities variation from 40% to 98% RH.

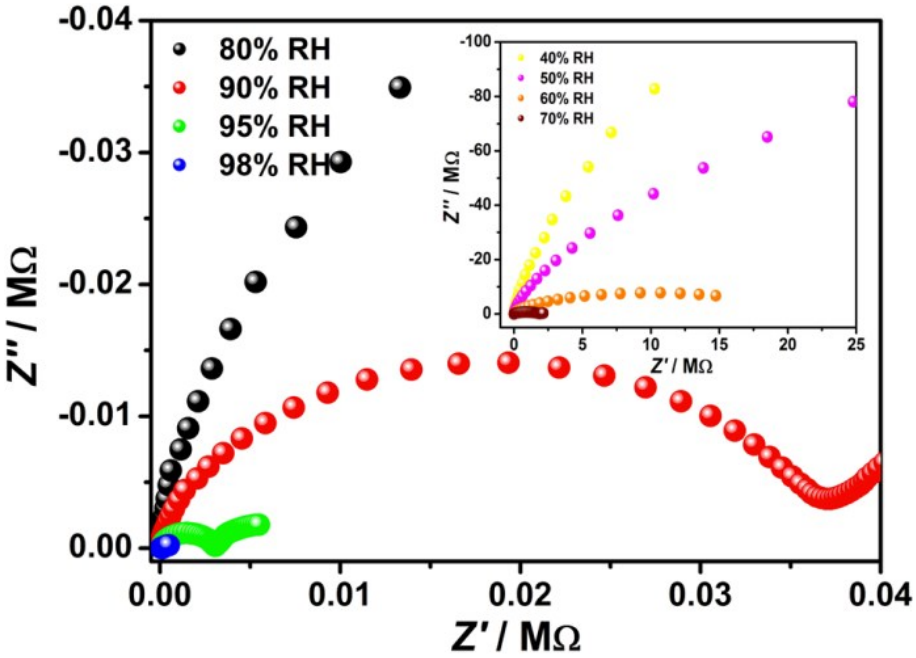

Figure S59. Nyquist plots from AC impedance data of UiO-66-NH_2-IM@PP membrane at 30 °C and different humidities variation from 40% to 98% RH.

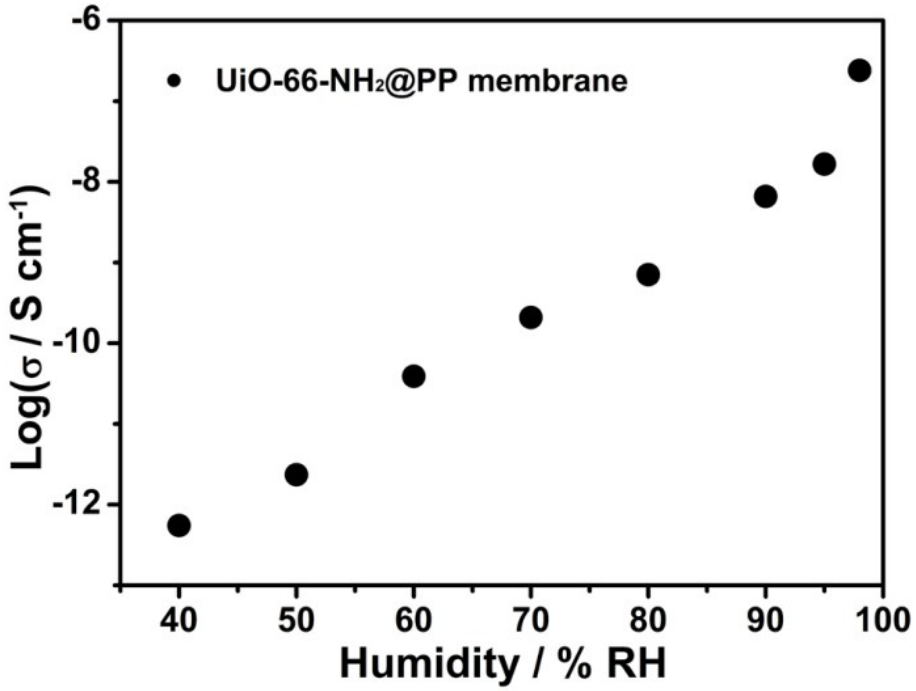

Figure S60. Log-scaled proton conductivities of UiO-66-NH_2@PP membrane at 30 °C and different humidities variation from 40% to 98% RH.

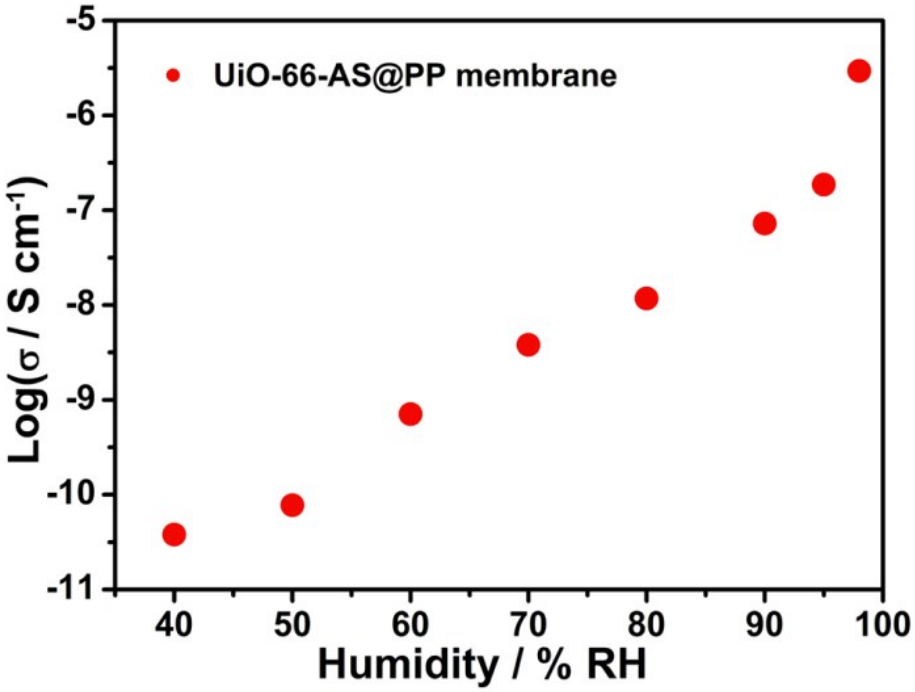

Figure S61. Log-scaled proton conductivities of UiO-66-AS@PP membrane at 30 °C and different humidities variation from 40% to 98% RH.

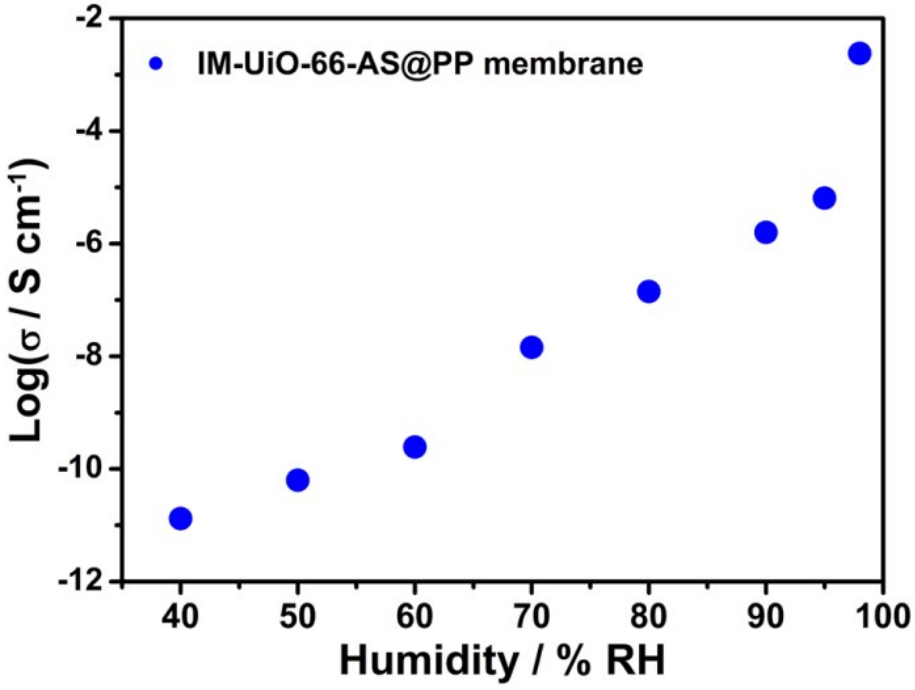

Figure S62. Log-scaled proton conductivities of IM-UiO-66-AS@PP membrane at 30 °C and different humidities variation from 40% to 98% RH.

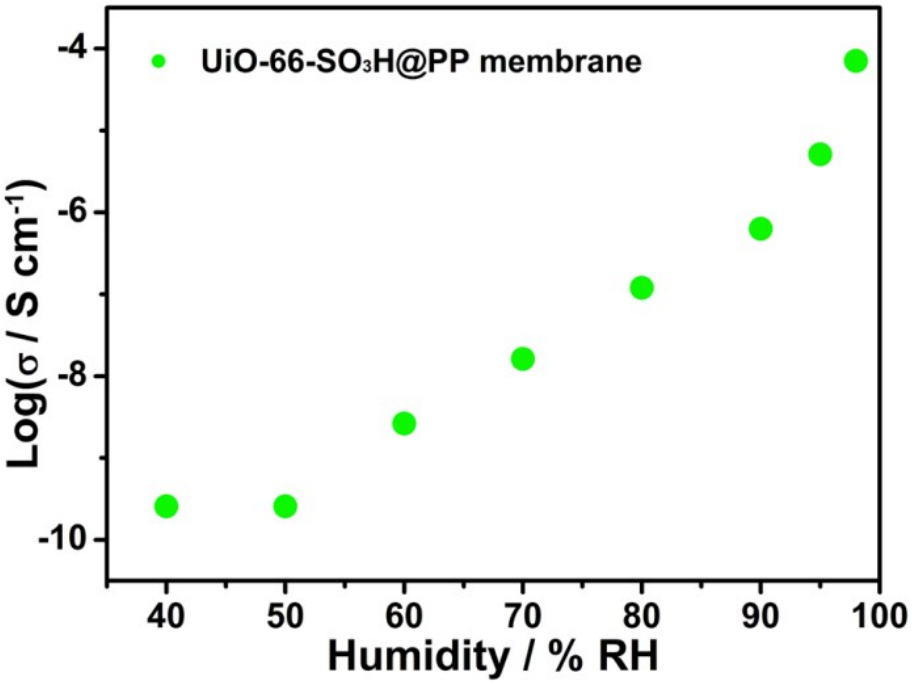

Figure S63. Log-scaled proton conductivities of UiO-66-SO_3H@PP membrane at 30 °C and different humidities variation from 40% to 98% RH.

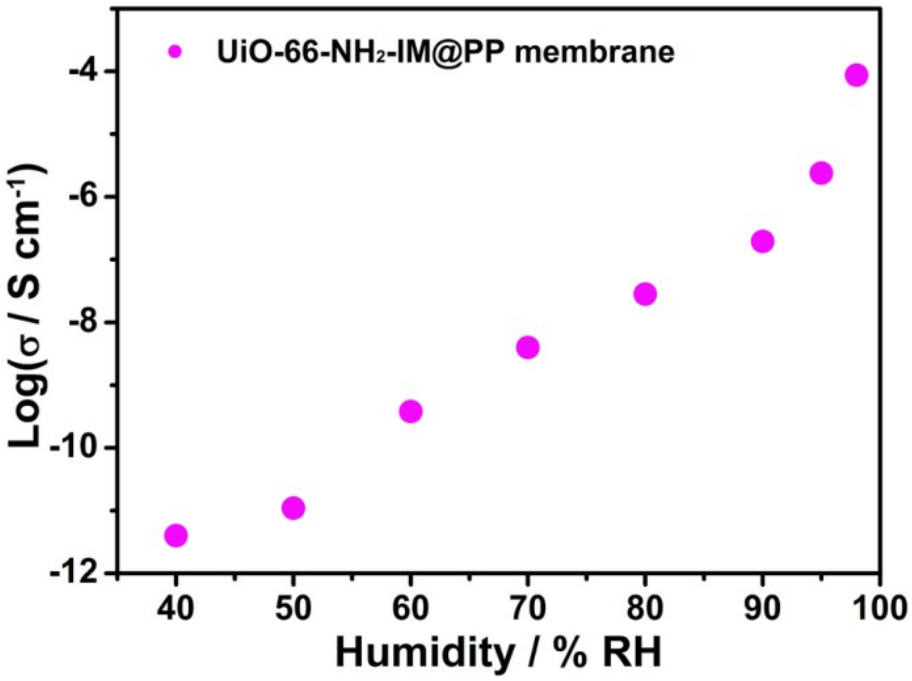

Figure S64. Log-scaled proton conductivities of UiO-66-NH_2-IM@PP membrane at 30 °C and different humidities variation from 40% to 98% RH.

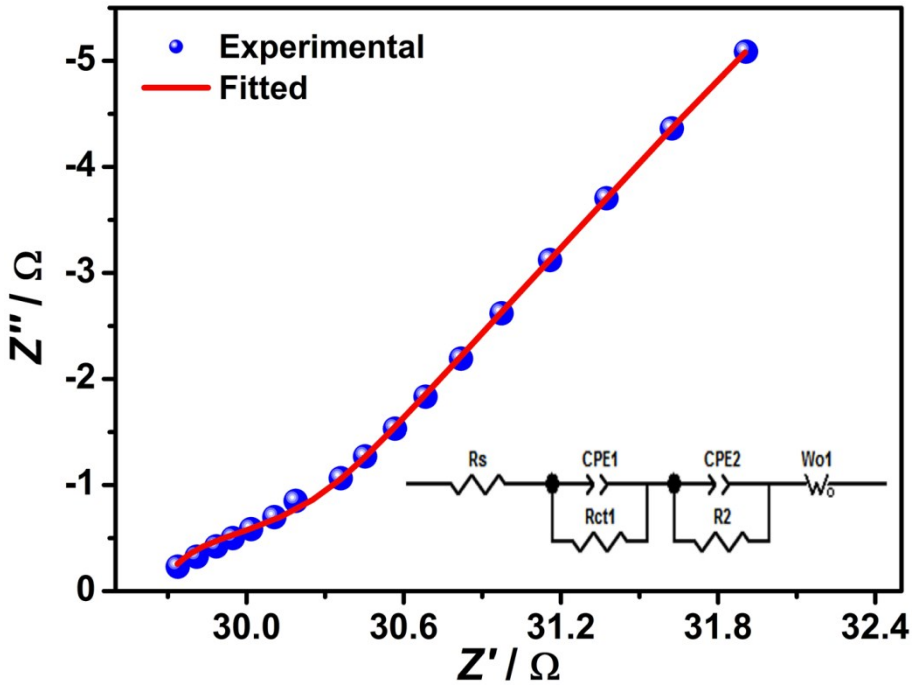

Figure S65. Fitting for the Nyquist plot at 80 °C and 98% RH of IM-UiO-66-AS@PP membrane, with circuit model used for the data fitting shown as an inset.

Table S7. The parameters for circuit model of IM-UiO-66-AS@PP membrane at 80 °C and 98% RH.

Element	Value
Rs	29.64
CPE1-T	1.331E-21
CPE1-P	3.65
Rct1	0.35755
CPE2-T	4.1168E-5
CPE2-P	0.77316
R2	1E+20
Wo1-R	1E-20
Wo1-T	5.408E-9
Wo1-P	3.409

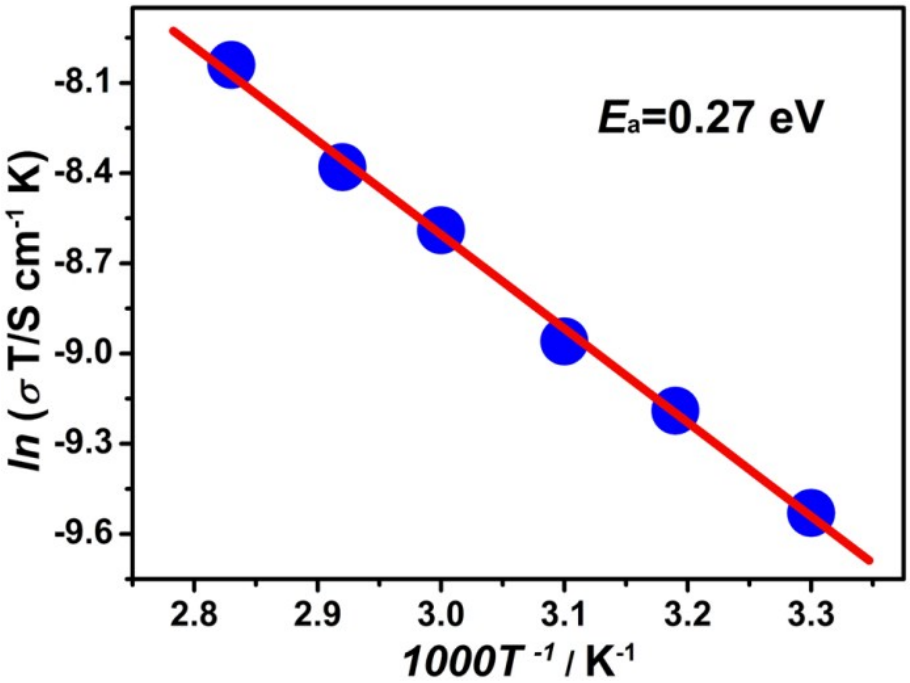

Figure S66. Arrhenius plot of UiO-66-NH_2@PP membrane (at the temperature range of 30-80 °C and 98% RH).

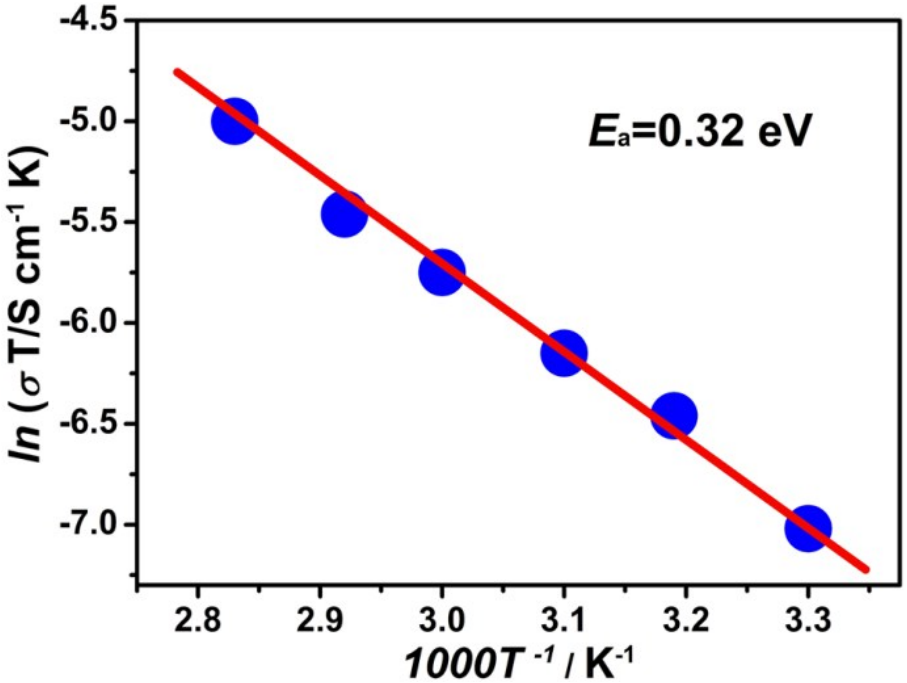

Figure S67. Arrhenius plot of UiO-66-AS@PP membrane (at the temperature range of 30-80 °C and 98% RH).

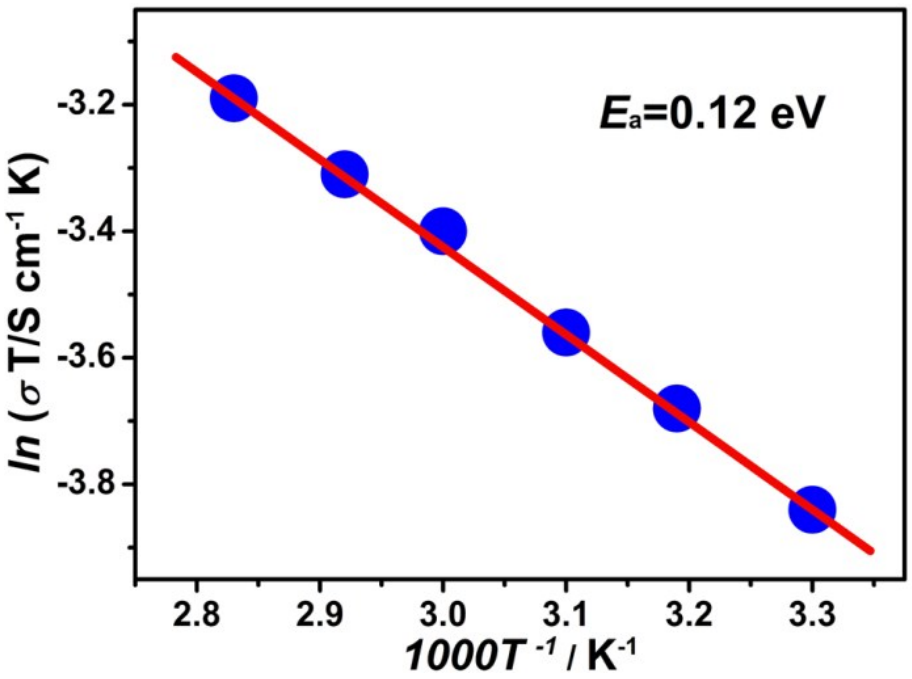

Figure S68. Arrhenius plot of UiO-66-SO_3H@PP membrane (at the temperature range of 30-80 °C and 98% RH).

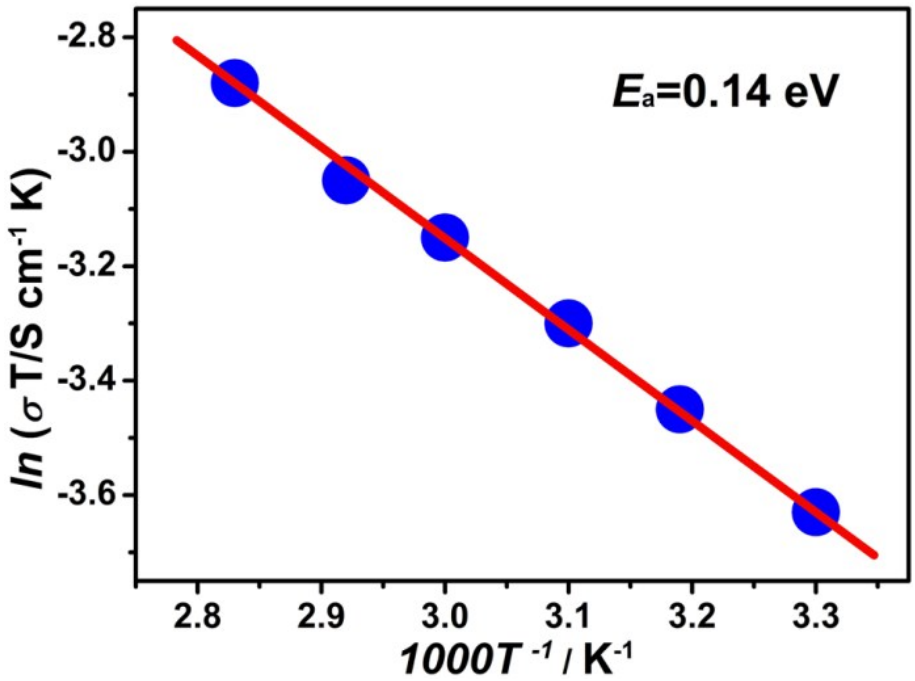

Figure S69. Arrhenius plot of UiO-66-NH_2-IM@PP membrane (at the temperature range of 30-80 °C and 98% RH).

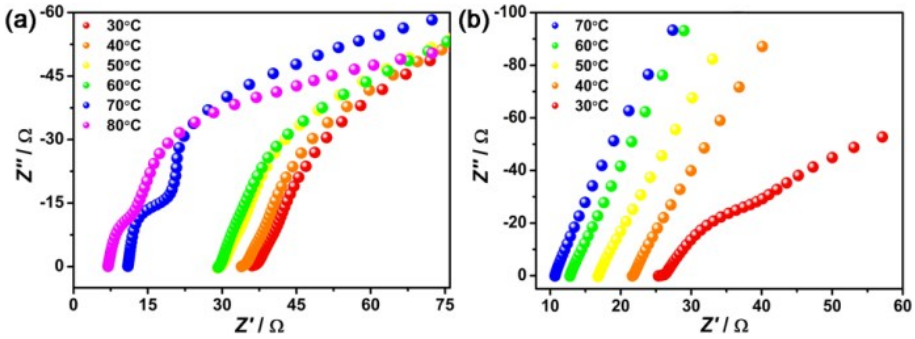

Figure S70. Nyquist plots from AC impedance data for the heating-cooling cycles of IM-UiO-66-AS@PP membrane under 98% RH. (a) the first heating cycle (30-80 °C), (b) the first cooling cycle (70-30 °C).

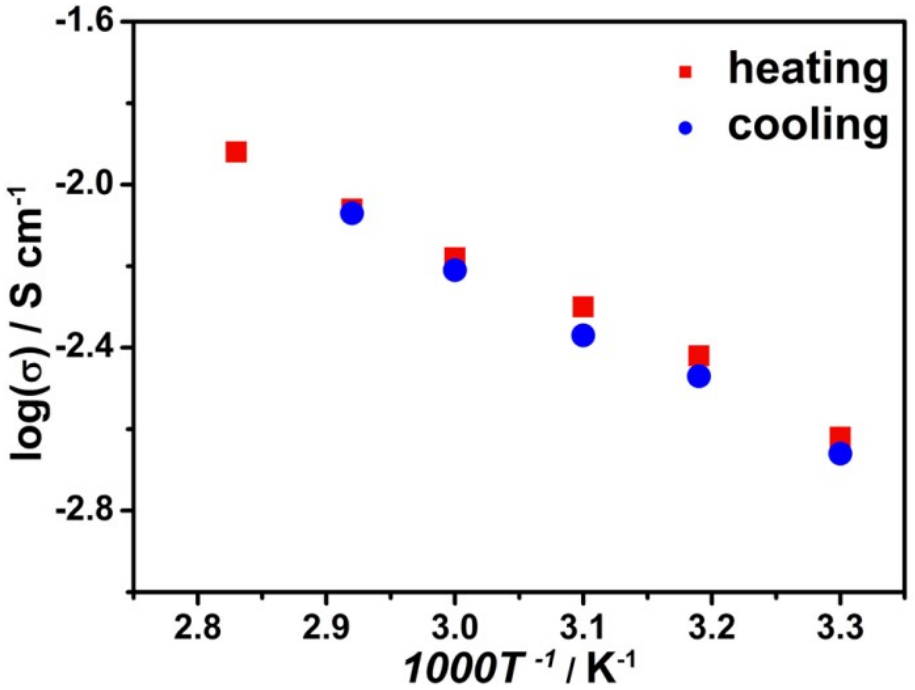

Figure S71. Log-scaled proton conductivities for the heating-cooling cycles of IM-UiO-66-AS@PP membrane at 98% RH.

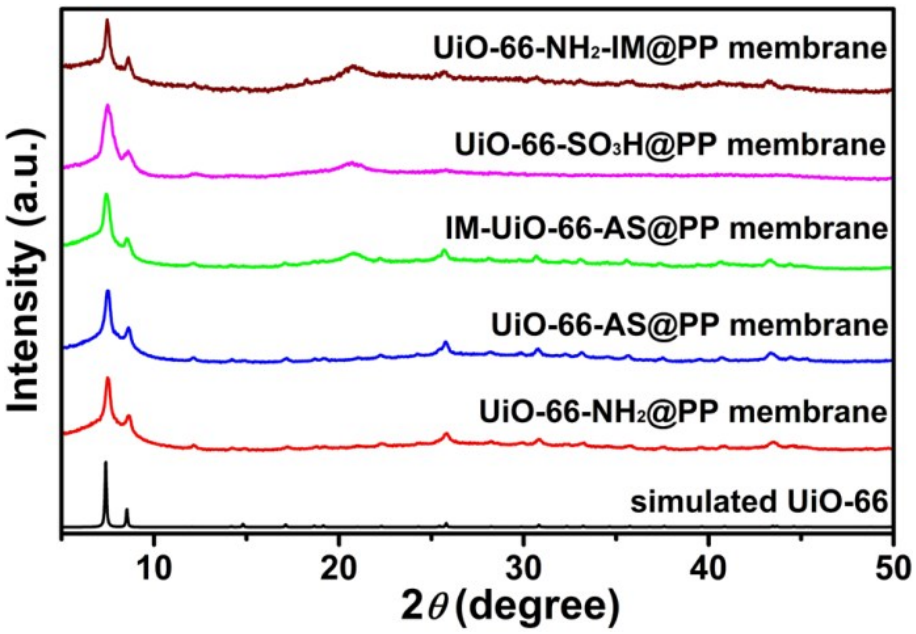

Figure S72. PXRD patterns of simulated UiO-66 (black) and UiO-66-NH_2@PP membrane (red), UiO-66-AS@PP membrane (blue), IM-UiO-66-AS@PP membrane (green), UiO-66-SO_3H@PP membrane (magenta) and UiO-66-NH_2-IM@PP membrane (wine) undergoing proton conduction measurements.

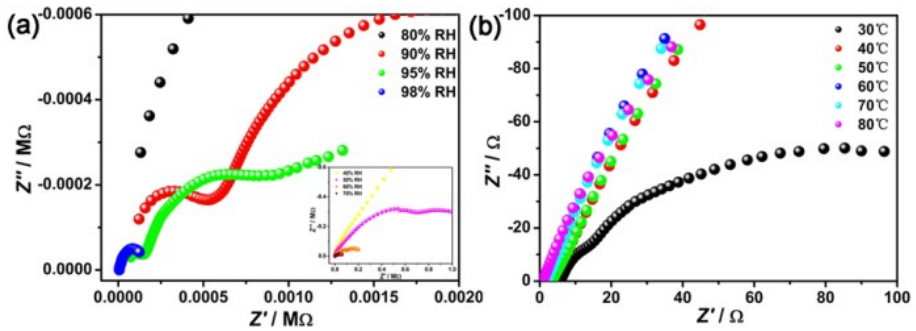

Figure S73. IM-UiO-66-AS@PP membrane (80 wt%): (a) Nyquist plots at 30 °C and different relative humidities from 40% to 98% RH. (b) Nyquist plots at 98% RH and different temperatures from 30 to 80 °C.

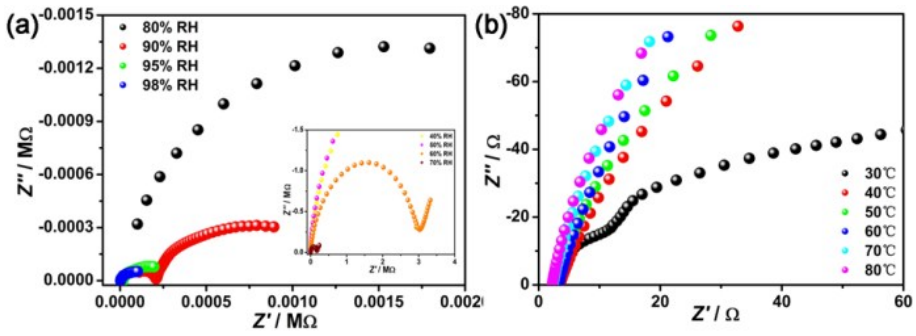

Figure S74. IM-UiO-66-AS@PP membrane (100 wt%): (a) Nyquist plots at 30 °C and different relative humidities from 40% to 98% RH. (b) Nyquist plots at 98% RH and different temperatures from 30 to 80 °C.

Table S8. Comparison of proton conductivity of IM-UiO-66-AS@PP membrane with some other representative MOFs-based hybrid membrane measured under hydrous condition.

Compounds	Conditions	σ (S cm^{-1})	E_a (eV)	Reference
IM-UiO-66-AS@PP membrane	80 °C, 98% RH	1.19×10^{-2}	0.32	This work
SPEEK/sul-MIL-7.5	75 °C, 100% RH	3.06×10^{-1}	/	58
CS/H_2SO_4@MIL-101-8	100 °C, 100% RH	9.5×10^{-2}	0.181	59
CS/H_3PO_4@MIL-101-6	100 °C, 100% RH	8.3×10^{-2}	0.175	59
CS/CF_3SO_3H@MIL-101-10	100 °C, 100% RH	9.4×10^{-2}	0.179	59
DNA@ZIF-8	75 °C, 97% RH	1.7×10^{-1}	0.86	60
MOF-801@PP-60	52 °C, 98% RH	1.84×10^{-3}	/	61
Nafion@CPO-25	50 °C, 100% RH	0.011	/	62
Nafion@MIL-53-Al	50 °C, 100% RH	0.010	/	62
2.5 wt% HKUST-1/Nafion	25 °C, 100% RH	1.8×10^{-2}	/	63
2 wt% UiO-66-SO_3H/Nafion	80 °C, 95% RH	0.17	/	64
1 wt% Zr-MOF-808-SO_3H/ Nafion	80 °C, 35% RH	2.98×10^{-3}	/	65
Nafion	60-80 °C, 98% RH	2×10^{-1}	/	66

Fuel Cell Assembly

The single cell was assembled for electrochemical evaluation, which contain a Pt/C anode, the flexible IM-UiO-66-AS@PP membrane and a Pt/C cathode. A uniform catalyst ink was prepared by physically blending the commercial Pt/C powders into a PTFE solution. Later, this ink was deposited onto a gas diffusion layer (GDL) by spraying technique with a Pt loading of 0.2 mg cm^{-2}, which served as both the anode and the cathode. The as-prepared flexible IM-UiO-66-AS@PP membrane was sandwiched between two electrodes by cold pressing way to obtain the single cell. The effective area of such single cell was 1 cm^2. The single cells were assessed at 80 °C on a fuel cell testing station (Greenlight G20, Canada) by an electrochemical workstation (Gamry Ref 3000) with humidified H_2 as the fuel and O_2 as the oxidant, respectively. The stability performance was measured at 70 mA cm^{-2} and 80 mA cm^{-2} at 80 °C and 98% RH.

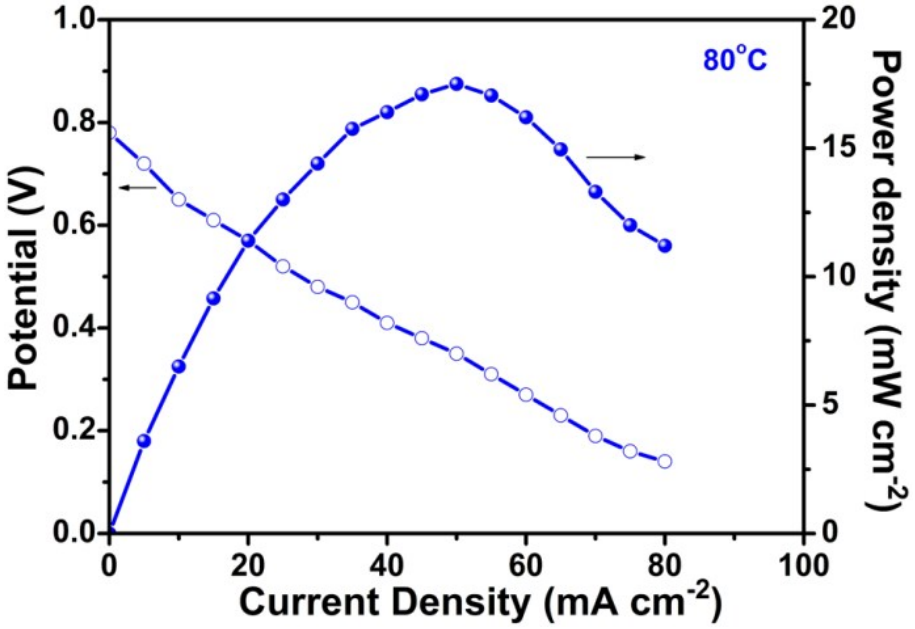

Figure S75. Performance of a H_2/O_2 fuel cell with IM-UiO-66-AS@PP membarne as the electrolyte at 80 °C and 98% RH. The blue hollow spheres and blue solid spheres represent current-voltage and current-power measurements, respectively.

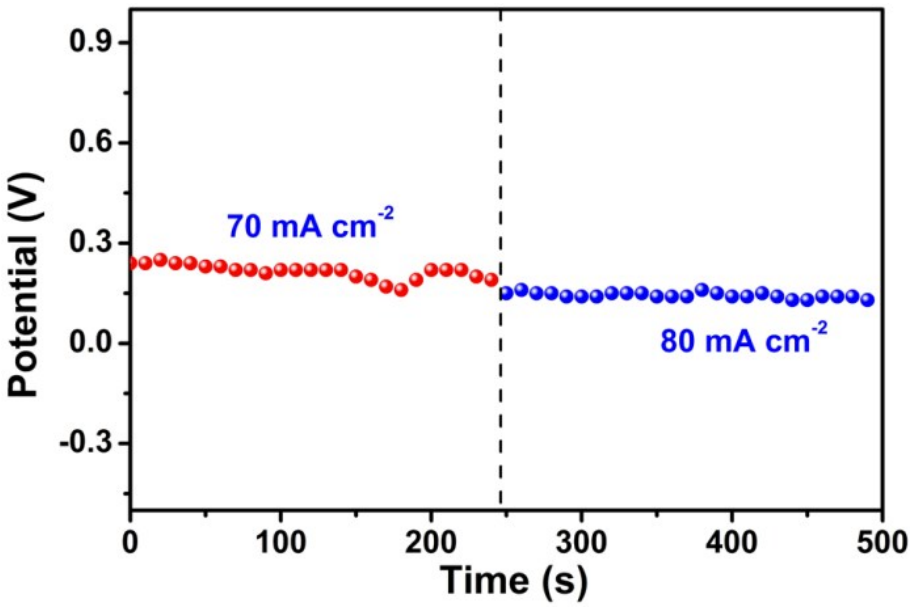

Figure S76. Stability of a H_2/O_2 fuel cell with IM-UiO-66-AS@PP membrane, measured at 70 mA cm^{-2} and 80 mA cm^{-2} at 80 °C and 98% RH.

Reference:

1. C. Gomes Silva, I. Luz, F. X. Llabrés i Xamena, A. Corma and H. García, *Chem. Eur. J.* **2010**, *16,* 11133.

2. F. Yang, H. Huang, X. Wang, F. Li, Y. Gong, C. Zhong and J.-R. Li, *Cryst. Growth Des.* **2015**, *15*, 5827.

3. S.-Y. Zhu and B. Yan, *Dalton Trans.* **2018**, *47*, 11586.

4. R. C. T. Slade, A. Hardwick and P. G. Dickens, *Solid State Ionics* 1983, **9,** 1093-1098.

5. T. Yamada, M. Sadakiyo and H. Kitagawa, *J. Am. Chem. Soc.* 2009, **131,** 3144-3145.

6. J. M. Taylor, R. K. Mah, I. L. Moudrakovski, C. I. Ratcliffe, R. Vaidhyanathan and G. K. H. Shimizu, *J. Am. Chem. Soc.* 2010, **132,** 14055-14057.

7. E. Pardo, C. Train, G. Gontard, K. Boubekeur, O. Fabelo, H. Liu, B. Dkhil, F. Lloret, K. Nakagawa, H. Tokoro, S.-i. Ohkoshi and M. Verdaguer, *J. Am. Chem. Soc.* 2011, **133,** 15328-15331.

8. A. Shigematsu, T. Yamada and H. Kitagawa, *J. Am. Chem. Soc.* 2011, **133,** 2034-2036.

9. C. Dey, T. Kundu and R. Banerjee, *Chem. Commun.* 2012, **48,** 266-268.

10. M. Sadakiyo, H. Ōkawa, A. Shigematsu, M. Ohba, T. Yamada and H. Kitagawa, *J. Am. Chem. Soc.* 2012, **134,** 5472-5475.
11. T. Kundu, S. C. Sahoo and R. Banerjee, *Chem. Commun.* 2012, **48,** 4998-5000.
12. T. Panda, T. Kundu and R. Banerjee, *Chem. Commun.* 2013, **49,** 6197-6199.
13. J. M. Taylor, K. W. Dawson and G. K. H. Shimizu, *J. Am. Chem. Soc.* 2013, **135,**1193-1196.
14. M. Wei, X. Wang and X. Duan, *Chem. Eur. J.* 2013, **19,** 1607-1616.
15. X. Liang, F. Zhang, W. Feng, X. Zou, C. Zhao, H. Na, C. Liu, F. Sun and G. Zhu, *Chem. Sci.* 2013, **4***,* 983-992.
16. M. Wei, X. Wang, J. Sun and X. Duan, *J. Solid State Chem.* 2013, **202,** 200-206.
17. X.-Y. Dong, R. Wang, J.-B. Li, S.-Q. Zang, H.-W. Hou and T. C. W. Mak, *Chem. Commun.* 2013, **49,** 10590-10592.
18. S. Kim, K. W. Dawson, B. S. Gelfand, J. M. Taylor and G. K. H. Shimizu, *J. Am. Chem. Soc.* 2013, **135,** 963-966.
19. S. S. Nagarkar, S. M. Unni, A. Sharma, S. Kurungot and S. K. Ghosh, *Angew. Chem. Int. Ed.* 2014, **53,** 2638-2642.
20. M. Zhu, Z.-M. Hao, X.-Z. Song, X. Meng, S.-N. Zhao, S.-Y. Song and H.-J. Zhang, *Chem. Commun.* 2014, **50,** 1912-1914.
21. Y. Liu, X. Yang, J. Miao, Q. Tang, S. Liu, Z. Shi and S. Liu, *Chem. Commun.* 2014, **50,** 10023-10026.
22. M. Sadakiyo, T. Yamada, K. Honda, H. Matsui and H. Kitagawa, *J. Am. Chem. Soc.* 2014, **136,** 7701-7707.
23. W. J. Phang, W. R. Lee, K. Yoo, D. W. Ryu, B. Kim and C. S. Hong, *Angew. Chem. Int. Ed.* 2014, **53***,* 8383-8387.
24. M.-L. Wei, J.-J. Sun and X.-Y. Duan, *Eur. J. Inorg. Chem.* 2014, **2014,** 345-351.
25. S.-S. Bao, K. Otsubo, J. M. Taylor, Z. Jiang, L.-M. Zheng and H. Kitagawa, *J. Am. Chem. Soc.* 2014, **136,** 9292-9295.
26. Y.-Q. Jiao, H.-Y. Zang, X.-L. Wang, E.-L. Zhou, B.-Q. Song, C.-G. Wang, K.-Z. Shao and Z.-M. Su, *Chem. Commun.* 2015, **51,** 11313-11316.

27. S.-N. Zhao, X.-Z. Song, M. Zhu, X. Meng, L.-L. Wu, S.-Y. Song, C. Wang and H.-J. Zhang, *Dalton. Trans.* 2015, **44,** 948-954.

28. X. Li, X. Sun, X. Li, Z. Fu, Y. Sua and G. Xu, *Cryst. Growth Des.* 2015, **15,** 4543-4548.

29. P. Barbosa, N. C. Rosero-Navarro, F.-N. Shi and F. M. L. Figueiredo, *Electrochim. Acta* 2015, **153,** 19-27.

30. P. Ramaswamy, N. E. Wong, B. S. Gelfand and G. K. H. Shimizu, *J. Am. Chem. Soc.* 2015, **137,** 7640-7643.

31. S. Sanda, S. Biswas and S. Konar, *Inorg. Chem.* 2015, **54,** 1218-1222.

32. X. Meng, S.-Y. Song, X.-Z. Song, M. Zhu, S.-N. Zhao, L.-L. Wu and H.-J. Zhang, *Chem. Commun.* 2015, **51,** 8150-8152.

33. W. J. Phang, H. Jo, W. R. Lee, J. H. Song, K. Yoo, B. Kim and C. S. Hong, *Angew. Chem. Int. Ed.* 2015, **54,** 5142-5146.

34. D. D. Borges, S. Devautour-Vinot, H. Jobic, J. Ollivier, F. Nouar, R. Semino, T. Devic, C. Serre, F. Paesani and G. Maurin, *Angew. Chem. Int. Ed.* 2016, **128**, 3987-3992.

35. C. Li, M. Sun, L. Xu, Y. Wang and J. Huang, *CrystEngComm* 2016, **18,** 596-600.

36. T. N. Tu, N. Q. Phan, T. T. Vu, H. L. Nguyen, K. E. Cordova and H. Furukawa, *J. Mater. Chem. A.* 2016, **4,** 3638-3641.

37. S. Pili, S. P. Argent, C. G. Morris, P. Rought, V. García-Sakai, I. P. Silverwood, T. L. Easun, M. Li, M. R. Warren, C. A. Murray, C. C. Tang, S. Yang and M. Schröder, *J. Am. Chem. Soc.* 2016, **138,** 6352.-6355

38. X.-M. Li, L.-Z. Dong, S.-L. Li, G. Xu, J. Liu, F.-M. Zhang, L.-S. Lu and Y.-Q. Lan, *ACS Energy Lett.* 2017, **2,** 2313-2318.

39. F. Yang, G. Xu, Y. Dou, B. Wang, H. Zhang, H. Wu, W. Zhou, J.-R. Li and B. Chen, *Nat. Energy* 2017, **2,** 877-833.

40. F.-M. Zhang, L.-Z. Dong, J.-S. Qin, W. Guan, J. Liu, S.-L. Li, M. Lu, Y.-Q. Lan, Z.-M. Su and H.-C. Zhou, *J. Am. Chem. Soc.* 2017, **139,** 6183-6189.

41. B. Joarder, J.-B. Lin, Z. Romero and G. K. H. Shimizu, *J. Am. Chem. Soc.* 2017, **139,** 7176-7179.

42. Y.-S. Wei, X.-P. Hu, Z. Han, X.-Y. Dong, S.-Q. Zang and T. C. W. Mak, *J. Am. Chem. Soc.* 2017, **139,** 3505-3512.

43. L. Zou, S. Yao, J. Zhao, D.-S. Li, G. Li, Q. Huo and Y. Liu, *Cryst. Growth Des.* 2017, **17,** 3556-3561.

44. X. Lai, Y. Liu, G. Yang, S. Liu, Z. Shi, Y. Lu, F. Luo and S. Liu, *J. Mater. Chem. A* 2017, **5,** 9611-9617.

45. K. Zhang, X. Xie, H. Li, J. Gao, L. Nie, Y. Pan, J. Xie, D. Tian, W. Liu, Q. Fan, H. Su, L. Huang and W. Huang, *Adv. Mater.* 2017, **29,** 1701804.

46. Y. Ye, W. Guo, L. Wang, Z. Li, Z. Song, J. Chen, Z. Zhang, S. Xiang and B. Chen, *J. Am. Chem. Soc.* 2017, **139,** 15604-15607.

47. N. E. Wong, P. Ramaswamy, A. S. Lee, B. S. Gelfand, K. J. Bladek, J. M. Taylor, D. M. Spasyuk and G. K. H. Shimizu, *J. Am. Chem. Soc.* 2017, **139,** 14676-14683.

48. T. He, Y.-Z. Zhang, H. Wu, X.-J. Kong, X.-M. Liu, L.-H. Xie, Y. Dou and J.-R. Li, *Chemphyschem* 2017, **18,** 3245-3252.

49. S. Kim, B. Joarder, J. A. Hurd, J. Zhang, K. W. Dawson, B. S. Gelfand, N. E. Wong and G. K. H. Shimizu, *J. Am. Chem. Soc.* 2018, **140,** 1077-1082.

50. S. Khatua, A. K. Bar, J. A. Sheikh, A. Clearfield and S. Konar, *Chem. Eur. J.* 2018, **24,** 872-880.

51. S. Wang, M. Wahiduzzaman, L. Davis, A. Tissot, W. Shepard, J. Marrot, C. Martineau-Corcos, D. Hamdane, G. Maurin, S. Devautour-Vinot and C. Serre, *Nat. Commun.* 2018, **9,** 4937.

52. S. Pili, P. Rought, D. I. Kolokolov, L. Lin, I. da Silva, Y. Cheng, C. Marsh, I. P. Silverwood, V. García Sakai, M. Li, J. J. Titman, L. Knight, L. L. Daemen, A. J. Ramirez-Cuesta, C. C. Tang, A. G. Stepanov, S. Yang and M. Schröder, *Chem. Mater.* 2018, **30,** 7593-7602.

53. P. G. M. Mileo, K. Adil, L. Davis, A. Cadiau, Y. Belmabkhout, H. Aggarwal, G. Maurin, M. Eddaoudi and S. Devautour-Vinot, *J. Am. Chem. Soc.* 2018, **140,** 13156-13160.

54. S. S. Park, A. J. Rieth, C. H. Hendon and M. Dincă, *J. Am. Chem. Soc.* 2018, **140,** 2016-2019.

55. Z. Sun, S. Yu, L. Zhao, J. Wang, Z. Li and G. Li, *Chem. Eur. J.* 2018, **24,** 10829-10839.

56. X. Wang, D. Lou, X. Lu, J. Wu, Y. Mu, Y. Yan, Q. Zhang and M. Bai, *Dalton Trans.* 2018, **47,** 9096-9102.

57. W.-W. Zhang, Y.-L. Wang, Q. Liu and Q.-Y. Liu, *Inorg. Chem.* 2018, **57,** 7805-7814.

58. Z. Li, G. He, Y. Zhao, Y. Cao, H. Wu, Y. Li and Z. Jiang, *J. Power Sources* 2014, **262,** 372-379.

59. X.-Y. Dong, J.-J. Li, Z. Han, P.-G. Duan, L.-K. Li and S.-Q. Zang, *J. Mater. Chem. A* 2017, **5,** 3464-3473.

60. Y. Guo, Z. Jiang, W. Ying, L. Chen, Y. Liu, X. Wang, Z.-J. Jiang, B. Chen and X. Peng, *Adv. Mater.* 2018, **30,** 1705155.

61. J. Zhang, H.-J. Bai, Q. Ren, H.-B. Luo, X.-M. Ren, Z.-F. Tian and S. Lu, *ACS Appl. Mat. Interfaces* 2018, **10,** 28656-28663.

62. C.-H. Tsai, C.-C. Wang, C.-Y. Chang, C.-H. Lin and Y. W. Chen-Yang, *Int. J. Hydrogen Energy* 2014, **39**, 15696-15705.

63. H. J. Kim, K. Talukdar and S.-J. Choi, *J. Nanopart. Res.* 2016, **18**, 47.

64. A. Donnadio, R. Narducci, M. Casciola, F. Marmottini, R. D' Amato, M. Jazestani, H. Chiniforoshan and F. Costantino, *ACS Appl. Mat. Interfaces* 2017, **9**, 42239-42246.

65. H. A. Patel, N. Mansor, S. Gadipelli, D. J. L. Brett and Z. Guo, *ACS Appl. Mat. Interfaces* 2016, **8**, 30687-30691.

66. H. S. Sasmal, H. B. Aiyappa, S. N. Bhange, S. Karak, A. Halder, S. Kurungot and R. Banerjee, *Angew. Chem. Int. Ed.*, 2018, **130**, 11060-11064.